Singularity theory of plane curves and its applications

J. Eggers[1] and N. Suramlishvili[1]

[1]*School of Mathematics, University of Bristol, Bristol, BS8 1TW, UK*

Abstract

We review the classification of singularities of smooth functions from the perspective of applications in the physical sciences, restricting ourselves to functions of a real parameter t onto the plane (x, y). Singularities arise when the derivatives of x and y with respect to the parameter vanish. Near singularities the curves have a universal *unfolding*, described by a finite number of parameters. We emphasize the scaling properties near singularities, characterized by similarity exponents, as well as scaling functions, which describe the shape. We discuss how singularity theory can be used to find and/or classify singularities found in science and engineering, in particular as described by partial differential equations (PDE's). In the process, we point to limitations of the method, and indicate directions of future work.

PACS numbers:

I. INTRODUCTION AND MOTIVATION

Over the past 20 years there has been a great deal of effort to describe and to classify singularities of partial differential equations (PDE's) [1–5], especially those arising in free surface flows. Such singularities can manifest themselves by a quantity which becomes discontinuous, as in a shock wave, or by certain quantities becoming infinite at a point in space and time, such as the pressure and the velocity at the point where a drop of liquid breaks into two [6].

On the other hand, "singularity theory" is a well-established and rigorous body of work in mathematics [7–11], which studies the singularities of *smooth* mappings. In the simplest case that the mapping is real-valued (then the mapping is often called a function), this is known as catastrophe theory. Singularities arise if the gradient (and/or higher derivatives) vanish; in the case of higher dimensional mappings singularities are points where the mapping is not invertible: at this point the Jacobian is no longer of the highest rank. If the mapping is the parametric representation of a curve or of a surface, at such points the curvature becomes infinite.

Yet applications of singularity or catastrophe theory to PDE's has until recently been more or less limited to optical caustics [12–15], which arise from singularities of the eikonal equation, which describes the motion of a wave front. There has also been some work applying similar ideas to shock waves [16–19], but there has been little effort to connect the phenomenon directly to the underlying PDE. Recently, we have pointed out that there is a wider connection between physical singularities and singularities of smooth mappings [20], with applications for example to the theory of viscous flow.

Singularities of smooth mappings can be understood as arising from geometry alone: the underlying function is smooth, but if a surface is seen under a certain angle, or a space curve is projected onto a plane, the resulting image may be singular. For example, the projection of the same space curve may be one-to-one from one direction, but self-intersecting from another. As we will see below, at the boundary between the two the curve forms a cusp singularity [20]. This is exactly the same singularity [20, 21] that is produced on the surface of a viscous liquid forced from inside the fluid. From the geometrical perspective it seems natural that wave propagation, which comprises caustics and shock waves, should be describable by singularity theory, since they involve deformation of the original wave front

along characteristics. It is remarkable that similar ideas can be applied to viscous motion as well.

In this review, we begin by outlining the basis of singularity theory for general mappings $f : \mathbb{R}^n \to \mathbb{R}^p$, but then focus on the special case of $n = 1$ and $p = 2$, which corresponds to a parametric representation of a plane curve. Within the framework of plane curves $(x(t), y(t))$, we illustrate how to classify the different fundamental singularities, known as "germs". The goal is to find all singularities up to a certain order which are not equivalent to one another, i.e. which cannot be transformed into one another by smooth transformations. In each case we investigate what happens if the germ is deformed locally in a smooth manner. Physically, this may happen in an infinity of different ways; however, each germ only has a finite number of parameters which determine the deformations completely, up to smooth transformations. The representation of such a minimal description is called a "miniversal unfolding". In the appendix we present the complete catalogue of singularities and unfoldings up to fourth order.

The neighborhood of singularities is often scale-invariant, so we place particular emphasis on the self-similar properties of unfoldings. This reduces the number of parameters further, in that unfoldings only differ by a scale transformation. With the scale transformation is associated a set of similarity exponents and scaling functions. Singularities of higher order may exhibit different types of scaling behavior in different regions of parameter space.

In the section on applications, we illustrate how the theory can be applied to singular solutions of PDE's. We begin with the simplest, and most thoroughly developed applications which use catastrophe theory. In that case the curve in question is defined implicitly by a scalar-valued "action" or "potential". The curve is either the front of a wave which propagates in the plane, or the profile of a hydrodynamic variable in one dimension. The description using the action variable reveals the close analogy between caustics (singularities of a wave front) and shocks (discontinuities in a hydrodynamic field variable).

For the remainder of the applications, we consider curves which can in general not be written in terms of a potential; physically the curves are most often free surfaces, such as the surface bounding a liquid. We present examples where the equations of fluid mechanics can be solved in terms of a (conformal) mapping, which usually guarantees the existence of a smooth mapping of the interface. Sometimes the solution to the mapping can be given explicitly, which can then be analyzed using the catalogue given above, which serves as a

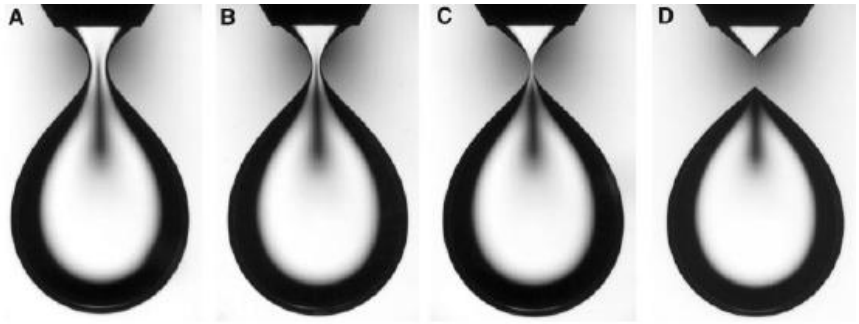

FIG. 1. The breakup of a drop of water (small viscosity) in a very viscous environment [22]. Between C and D, the water drop breaks and separates from the nozzle.

guide to the physical phenomena which can occur. If (as it is often the case) the solution to the mapping cannot be given explicitly, no predictions can be made, but singularity theory can still tell us what possibilities to look for. We also give cautionary examples where in spite of the existence of a mapping, singularities are not described by the theory, because the singularity arises at points where the mapping fails to be smooth.

Let us illustrate the approach with a physical example: the breakup of a drop of water inside another fluid of much larger viscosity, as shown in Fig. 1. In the limit that the viscosity of the drop can be neglected, the equation for the local drop radius $h(x,t)$ (here x is the position along the axis and t time) becomes very simple [5, 22], if one considers the motion close to pinch-off, where h goes to zero:

$$\frac{\partial h}{\partial t} = -\frac{\gamma}{2\eta}. \tag{1}$$

Here γ is the surface tension, and η the viscosity of the outer fluid. There is no spatial derivative (the equation is not a PDE, as one would expect) and is trivial to solve:

$$h(x,t) = h_0(x) - \frac{\gamma t}{2\eta}, \tag{2}$$

where $h_0(x)$ is the initial profile at $t = 0$.

As illustrated in Fig. 2, pinch-off occurs when $h(x,t)$ first touches the x-axis, which will be at the minimum of $h_0(x)$, determined by $h_0'(x_0) = 0$. Our task is thus to classify the minima of the arbitrary smooth function $h_0(x)$; this is of course an elementary problem, but serves our purpose of illustrating the key concepts presented in this review. At the minimum, the mapping $x \to h_0$ does not have its highest rank (which is 1), and hence represents a singularity (or critical point).

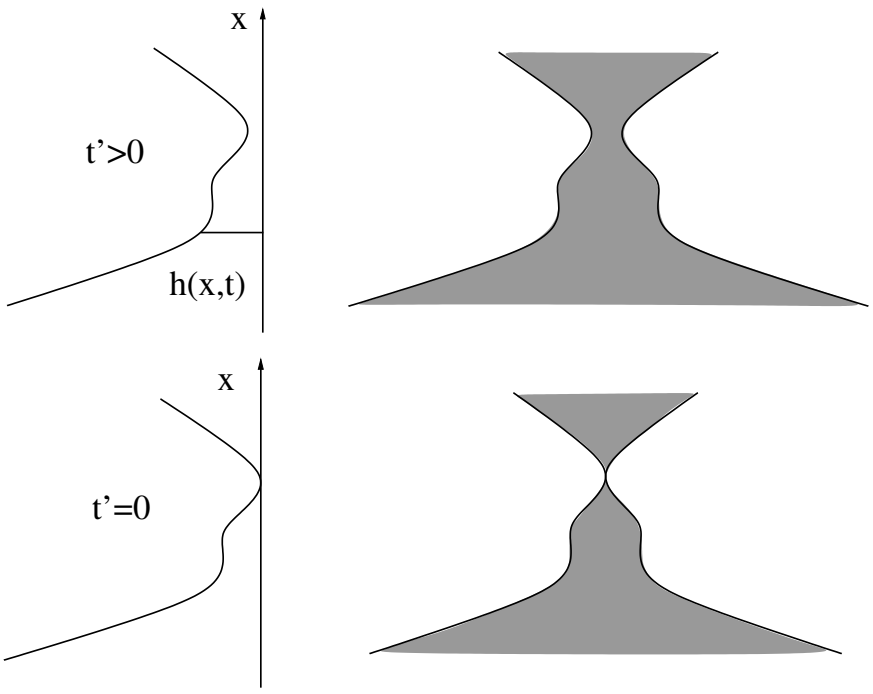

FIG. 2. A simple model for the experimental sequence of drop pinch-off shown in Fig. 1. The sequence on the right shows the neighborhood of the pinch-off region, with the fluid shown as shaded; at $t' \equiv t_0 - t = 0$, the radius goes to zero. In the sequence on the left it is shown how the dynamics are generated by a simple *shift* of the profile at constant rate, as given by (2).

The simplest local behavior satisfying $h_0' = 0$ is

$$h_0 = x^2, \tag{3}$$

which is the germ of the singularity; by a shift of the coordinate system, we can assume that the minimum is at $x = 0$. We now ask what happens to the singularity when the profile is perturbed slightly (as it is inevitable in a physical situation). This perturbation can happen in infinitely many ways; expanding into a power series, the perturbed profile becomes

$$h_0 = x^2 + \epsilon_1 x + \epsilon_3 x^3 + \dots. \tag{4}$$

We only investigate the neighborhood of the singularity, assuming the perturbation to be small, i.e. only terms linear in the parameters ϵ_i are considered. The coefficient of the quadratic term (the germ) can always be normalized to unity, so it was omitted. We would like to know if there is a qualitative change in the behavior near the minimum, which cannot be undone by a *smooth* transformation. First, all perturbations of higher order than the germ

can be removed by the transformation

$$\tilde{x}^2 = x^2 + \epsilon_3 x^3 + \dots$$

called a right transformation, because it affects the independent variable. It can be written as

$$\tilde{x} = \phi(x) \equiv x\left(1 + \epsilon_3 x + \dots\right)^{1/2}, \tag{5}$$

where $\phi(x)$ is locally smooth and invertible, a so-called diffeomorphism. As a result, we obtain to linear order $h_0 = \tilde{x}^2 + \epsilon_1 \tilde{x}$.

In a second step, the coefficient ϵ_1 can be eliminated as well by the shift $\tilde{x} \to \tilde{x} - \epsilon_1/2$, leading to the universal form $h_0 = \tilde{x}^2$ of the quadratic germ. We say the quadratic germ is *structurally stable*, since it remains unchanged under a perturbation (up to smooth transformations).

Before we go on, we point out that the germ (3) is also associated with certain scaling properties near the singularity. In fact, the Laplace pressure diverges for $h \to 0$, hence in spite of its apparent simplicity pinch-off is a very violent event. We write the profile in the self-similar form [5]

$$h(x,t) = t'^{\alpha} f\left(\frac{x}{t'^{\beta}}\right), \tag{6}$$

where $t' = t_0 - t$ is the time distance to the singularity. From (2) and the above analysis we conclude that the time-dependent profile can be written

$$h(x,t) = \frac{\gamma}{2\eta}\left(t' + ax^2\right) \equiv \frac{\gamma}{2\eta} t' f(\xi), \quad \xi = \frac{x}{t'^{1/2}}, \tag{7}$$

where the *similarity profile* is $f(\xi) = 1 + a\xi^2$. Thus the quadratic germ is associated with scaling exponents $\alpha = 1$ and $\beta = 1/2$.

The germ of next higher order is x^3, but only $h_0 = x^4$ corresponds to a minimum (known as the A_3 catastrophe [23]). The scaling exponents of the germ are now $\alpha = 1$, $\beta = 1/4$. Again, one can consider perturbations of any order $\epsilon_i x^i$, which for $i > 5$ can be removed by a transformation analogous to (5). A shift $x \to x - \epsilon_3/4$ then removes the term $\epsilon_3 x^3$. However, the remaining two terms cannot be removed by a smooth transformation [23], and we are left with the miniversal unfolding:

$$h_0 = x^4 + \epsilon_1 x + \epsilon_2 x^2. \tag{8}$$

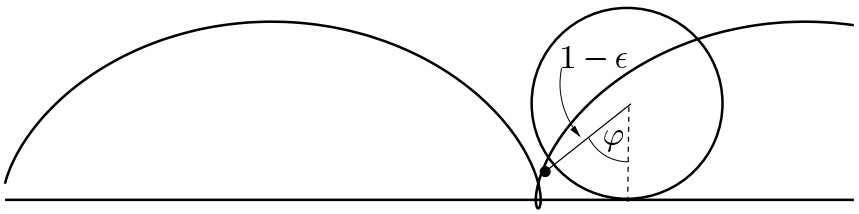

FIG. 3. A trochoid is the trajectory of a point fixed on (or external to) a rolling disk, shown here for $\epsilon < 0$.

This describes the neighborhood of the singularity with a minimum number of parameters (again, up to smooth transformations). This minimum number is also known as the *codimension*, and so $\mathrm{cod}(A_3) = 2$. Clearly, this higher order singularity is no longer stable: As soon as ϵ_1 or ϵ_2 are non-zero, the order of the minimum is quadratic, and one returns to (3). Physically, this means that even if one starts from a profile with quartic minimum, small perturbations will drive the dynamics away from the corresponding singular behavior, and instead pinch-off is described by (7). A stability analysis of the quartic case reveals that the corresponding similarity solution is unstable [5].

Of course, one should not jump to the conclusion that all singularities can be classified in this way. For the approach to bear fruit, one needs to describe the solution in terms of a smooth mapping, which in general is not guaranteed, or may even be the exception. Take for example a problem superficially similar to that shown in Fig. 1, a drop of very viscous liquid breaking up inside air (whose effect can be neglected) [5, 24, 25]. Now the viscous flow is inside the drop, rather than in the exterior. We do not give the solution here, but mention only that in Lagrangian coordinates (following trajectories of the flow), the equation of motion can in fact be written in a way similar to (1), but with an additional, nonlocal term, whose value depends on on integral over the whole profile. The solution near pinch-off can once more be written in the self-similar form (6), with exponent $\alpha = 1$. For the axial exponent β one also obtains a sequence β_i, whose values depend on the order of the minimum of the profile; only the first of these exponents corresponds to a stable solution [26]. However, the β_i are now solutions of a transcendental equation, and assume irrational values. It is clear that such values cannot result from an expansion in power laws, which only yield rational values.

The example discussed so far only considers curves which can be represented as a graph.

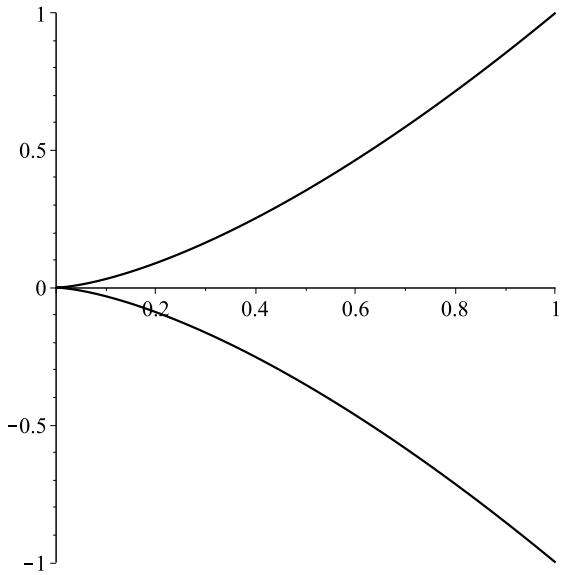

FIG. 4. The cusp (t^2, t^3)

However, for most of this review we will consider general smooth curves, which can be represented in parametric form $(x(t), y(t))$. In particular, this includes the case of self intersection, which leads to a particular type of cusp singularity, an example of which is shown in Fig. 3. As a disk is rolling on a flat surface, we are looking at the trajectory produced by a point attached to the disk, where ϵ is the distance from the perimeter.

Thus the trajectory is a superposition of the translation and the rotation of the rolling disk, leading to:

$$x = \varphi - (1-\epsilon)\sin\varphi, \quad y = 1 - (1-\epsilon)\cos\varphi. \tag{9}$$

Expanding about $\varphi = 0$ for finite ϵ we obtain

$$x = \epsilon\varphi + (1-\epsilon)\varphi^3/6 + O(\varphi^5), \quad y = \epsilon + (1-\epsilon)\varphi^2/2 + O(\varphi^4),$$

the first equation of which suggests $\varphi^2 \propto \epsilon$. Expanding consistently, we obtain

$$x = \epsilon\varphi + \varphi^3/6, \quad y = \epsilon + \varphi^2/2. \tag{10}$$

In Fig. 3 the case $\epsilon < 0$ is shown, for which the trajectory has a self-intersection; for $\epsilon > 0$ there is no intersection. In the critical case $\epsilon = 0$ a cusp appears at $\varphi = 0$, where $x_\varphi = y_\varphi = 0$, i.e. the mapping is non-invertible; the cusp has a characteristic 2/3 power law exponent, see Fig. 4. The unfolding (10) describes how a small perturbation transforms the

cusp into a regular curve. The general theory described below shows that the miniversal unfolding contains a single parameter only, so (10) captures all possible shapes up to smooth perturbations. For example, we could have considered the much more general problem of a disk which is not perfectly circular, and whose shape is described by any number of parameters. The above result implies that this does not lead to shapes which are any more general than (10), but that all shapes close to a cusp are described by this form.

II. GENERAL THEORY

We begin with a description of the general theory for arbitrary mappings, introducing only the key definitions. All the actual development of the theory will concern plane curves only. We have seen that a smooth mapping (which is C^∞, differentiable infinitely many times) $f : \mathbb{R}^n \to \mathbb{R}^p$ is able to describe singular behavior. By a singularity we mean that at a point in $\mathbb{R}^n$ (which we can take as the origin), the Jacobi matrix $Jf(0)$ no longer has full rank, i.e. $\mathrm{rk}_0(f) < \min(n, p)$. In the case of a plane curve $\mathbf{x}(\varphi)$ this means that $x'(0) = y'(0) = 0$. Otherwise (if f were *not* singular) we can introduce a change of coordinates which turns f into a trivial map (which has nothing singular about it). A change of coordinates means that there are smooth, invertible maps (or diffeomorphisms) $\phi : \mathbb{R}^n \to \mathbb{R}^n$ and $\psi : \mathbb{R}^p \to \mathbb{R}^p$ such that the function $g : \mathbb{R}^n \to \mathbb{R}^p$, defined by

$$g = \psi \circ f \circ \phi^{-1}, \tag{11}$$

is the representation of f in the new coordinate system.

Now if $n \geq p$ (the function f is a submersion), there is a coordinate transformation (11) such that [27]

$$g(x_1, \ldots, x_p, x_{p+1}, \ldots, x_n) = (x_1, \ldots, x_p),$$

i.e. g becomes a projection onto the lower dimensional space. If on the other hand $n < p$ (the function f is an immersion), a coordinate transformation will produce

$$g(x_1, \ldots, x_n) = (x_1, \ldots, x_n, 0, \ldots, 0)),$$

i.e. g is the identity on $\mathbb{R}^n$. For example, any nonsingular plane curve can be written as $x(\varphi) = \varphi$, $y(\varphi) = 0$, after the transformation.

We now apply the same idea to functions f which are singular, i.e. $\mathrm{rk}_0(f) < \min(n,p)$, aiming to classify maps *up to smooth, invertible deformations* as described by (11). We call two maps f, g related through (11) left-right, or $\mathcal{A}$-equivalent. The map ϕ describes a right transformation, ψ the left transformation. From now on, we will refer to a given function only as a representation of an equivalence class of the transformation.

Another crucial concept is to ask how f behaves under small perturbations. Clearly, if f is not singular, it will still be non-singular if a small perturbation has been applied to it; such a function is called stable. If on the other hand f is singular, a typical perturbation will remove the singularity. Thus the character of a singularity and the behavior of a function under perturbations are intimately connected. The ways in which a function may be perturbed in some sense characterizes the singularity.

To describe perturbations to a (singular) function $f : \mathbb{R}^n \to \mathbb{R}^p$ more formally, we introduce the family of smooth mappings $F : \mathbb{R}^n \times \mathbb{R}^d \to \mathbb{R}^p$ such that $F(\mathbf{x}, \mathbf{u} = 0) = f(\mathbf{x})$. Then f is called the singularity germ, and for any value $\mathbf{u} = (u_1, \ldots, u_d)$ of the *control parameters*, $\mathbf{x} \to F(\mathbf{x}, \mathbf{u})$ is called an unfolding of the singularity. In a typical physical situation, there is an arbitrary number of ways in which the system can be perturbed, so d may be any number. However, two different unfoldings will in general be equivalent; the minimum number of parameters needed to describe all possible unfoldings of a singularity is called the codimension: $\mathrm{cod}(f)$. A family of functions with this minimum number of parameters is called the miniversal unfolding. In perturbing the system, $\mathbf{u}$ will be considered infinitesimally small, i.e. we consider only terms linear in u_i, and quadratic terms will be dropped.

The codimension depends on the type of singularity, and will be greater if higher derivatives of f vanish; more precisely, f has a singularity of type S_k if $\mathrm{rk}(f) = \min(n,p) - k$, where k is called the deficiency of the singularity; the deficiency of a regular point is 0. The deformation of a singularity germ around the bifurcation center $\mathbf{u} = 0$ produces an unfolding such that the singularity is either completely removed or the deficiency is reduced. The variations of control parameters in an unfolding determine all possible topologies and bifurcations of the family of maps and their corresponding shapes.

To determine the points where the unfolding changes character, we have to determine the set of points where the mapping $\mathbf{x} \to F(\mathbf{x}, \mathbf{u})$ (at fixed value of the control parameters $\mathbf{u}$) is singular. If we define by $\mathrm{rk}_{x,u}(JF)$ the rank of the Jacobian of this mapping, the singular

set of the map is defined as:

$$\Sigma F = \{(x,u) \in \mathbb{R}^n \times \mathbb{R}^d \mid \mathrm{rk}_{x,u}(JF) < \min(n,p)\}. \tag{12}$$

In (10), ΣF consists of the single point $(0,0)$; namely, for $\epsilon = 0$ the curve becomes singular at $\varphi = 0$ to form a cusp. At this value of the control parameter ϵ, the topology changes; the set consisting of the single point $\epsilon = 0$ is called the bifurcation set. More generally, the bifurcation set (sometimes referred to as the discriminant) is defined as the projection of the singular set onto control space:

$$\Delta_F = \pi_F(\Sigma F) = \{u \in \mathbb{R}^d \mid \text{for such } x \in \mathbb{R}^n \text{ that} (x,u) \in \Sigma F\}. \tag{13}$$

If a parameter $u = u_0$ does not belong to the discriminant ($u \notin \Delta_F$), then there exists a neighborhood of u_0 such that the number and character of singular points of mappings $F(x,u)$ is same as for $F(x,u_0)$. Hence Δ_F divides the control space into connected regions where number of singular points is constant. Returning to the example of the cusp singularity, the discriminant is the set $\epsilon = 0$, which divides the control space into the area $\epsilon < 0$ with self-intersecting plane curves and $\epsilon > 0$ with regular non-intersecting curves. The two areas are connected at $\epsilon = 0$ where the curve exhibits the cusp singularity.

III. SINGULARITIES OF PLANE CURVES

We now apply the above ideas to the special case of plane curves [28–30], ($n = 1$ and $p = 2$), defined by two smooth functions $x(t), y(t)$. A singularity arises if $x'(0) = y'(0) = 0$. Our aim is to classify different types of singularities of plane curves, and to calculate their miniversal unfoldings. All functions are considered up to smooth transformations ($\mathcal{A}$-equivalence) only.

A first important observation is that any smooth mapping is $\mathcal{A}$-equivalent to a polynomial [28], so we can write

$$x = \sum_{i=m}^{\infty} a_i t^i, \quad y = \sum_{i=n}^{\infty} b_i t^i. \tag{14}$$

Without loss of generality, we can assume that $m < n$, since for $m = n$ the left transformation $\tilde{y} = b_1 x - a_1 y$ will eliminate the leading term in the expansion of y. The integer m is called the multiplicity of the singularity. In a second step, we use the right transformation

$$a_m \tilde{t}^m = a_m t^m + a_{m+1} t^{m+1} + \ldots \tag{15}$$

to obtain $x = \tilde{t}^m$. Writing

$$\tilde{t} = t\,(1 + a_{m+1}t/a_m + \dots)^{1/m} = t + a_{m+1}/(ma_m)t^2 + \dots$$

it is clear that this is a smooth and invertible transformation, and thus (14) is $\mathcal{A}$-equivalent to

$$x(t) = t^m, \quad y(t) = \sum_{i \geq n} c_i t^i, \quad \text{where } n > m. \tag{16}$$

Clearly, we can assume that $m \geq 2$, otherwise $x'(0) \neq 0$. A complete classification exists for germs of simple singularities, i.e. singularities with multiplicity $m \leq 4$, which is reported in Appendix B. In the case of simple singularities it can be assumed that the coefficients c_i are either 0 or unity, indicating whether a certain power is present. However, for singularities of higher order the prefactor cannot necessarily be normalized: in this so-called modular case [8] two singularities with two different non-zero values of c_i will not be $\mathcal{A}$-equivalent.

A complete classification for germs of arbitrary order does not exist. To bring out the basic principles of a classification, we begin the simplest but also most common (and probably most important) case of each component being described by a single power law exponent: monomial germs. However, the structure of a singularity can be affected considerably by the presence of powers of higher order, which cannot be eliminated. To illustrate this we will also consider the case of a second monomial.

A. Monomial germs

Monomial germs are those whose components consist of a single power:

$$(t^m, t^n), \quad \text{hcf}(m, n) = 1. \tag{17}$$

We can assume that the integers m, n do not have a common factor, j, because if they had, we could define $\tilde{t} = t^j$. The pair (m, n) are called the Puiseux exponents $\beta_0 = m$ and $\beta_1 = n$ of the singularity, which are introduced more generally in Appendix A. As there is only a single Puiseux exponent in the second component, the so-called genus is $g = 1$. This is the simplest case of the Puiseux sequence of characteristic exponents, which is calculated as in (A2) below, and is defined for any singularity. Two simple examples of monomial germs, to be encountered frequently below, are the cusp germ (t^2, t^3), which was shown in Fig. 4, and the "swallowtail" germ (t^3, t^4).

B. Unfoldings

We are now in a position to calculate the miniversal unfoldings of monomial singularities, and thus the codimension. The most general unfolding is

$$\left(t^m + \sum_l \epsilon_l t^l, t^n + \sum_l \mu_l t^l \right). \tag{18}$$

In the theory of unfoldings, only infinitesimal perturbations are considered, i.e. only terms linear in ϵ_i,μ_i. In a first step, we can eliminate all terms $\epsilon_i, i \geq m$, using the right transformation (15) as before.

Next we consider the left transformations

$$\tilde{x} = x, \quad \tilde{y} = y - \epsilon x^i y^j = y - \epsilon t^{im+jn} + O(\epsilon^2). \tag{19}$$

Then if $l = im + jn$, the choice $\epsilon = \mu_l$ eliminates the corresponding term; the elements $l = im + jn$ form a semigroup $S(f)$, generated by (m, n). For example, if the singularity f is the monomial germ $(m, n) = (3, 4)$, we have $S(f) \equiv < 3, 4 > = \{3, 4, 6, 7, 8, \dots\}$. Integers not contained in $S(f)$ form the set of gaps G, which here are $G = \{1, 2, 5\}$; the smallest integer in $S(f)$ above which there are no gaps is called the conductor c (here $c = 6$). Clearly, all coefficients μ_l corresponding to a power l in G *cannot* be eliminated by the transformation (19).

In a third step, some powers in the series expansion of $x(t)$ as well as of $y(t)$ can be eliminated by considering an infinitesimal shift of t. Clearly, this shift points in the direction tangent to the curve, and hence one speaks of generating the tangent space. In particular, we consider the infinitesimal right transformation $\tilde{t} = t - \epsilon(t)$, which generates

$$\tilde{x} = x(\tilde{t} + \epsilon) = x(\tilde{t}) + x'\epsilon(t) + O(\epsilon^2), \quad \tilde{y} = y(\tilde{t}) + y'\epsilon(t) + O(\epsilon^2). \tag{20}$$

Hence $\tilde{x} = x + mt^{m-1}\epsilon$, which means that all ϵ_i with $i \geq m - 1$ can be eliminated.

To eliminate terms from the expansion of $y(t)$ without interfering with $x(t)$, we need to generate a tangent space $(0, w_y)$. To this end, we consider the general transformation

$$w_x = \sum_{i,j} a_{ij} x^i y^j + x'\epsilon(t), \quad w_y = \sum_{i,j} b_{ij} x^i y^j + y'\epsilon(t), \tag{21}$$

and demand that $w_x = 0$. In the case of the germ (t^m, t^n), this condition leads to

$$\epsilon(t) = -\frac{a_{ij}}{m} t^{im+jn-m+1}.$$

Since we are considering terms to linear order only, we can eliminate each term separately. We obtain

$$w_y = \left(b_{ij} - a_{ij} \frac{n}{m} t^{n-m} \right) t^{im+jn}, \tag{22}$$

so in addition to the semigroup we can eliminate all powers of the form

$$t^{im+jn+n-m}, \quad i+j>0, \quad i,j \geq 0. \tag{23}$$

To summarize, the unfolding of a monomial germ contains at most the terms

$$\left(t^m + \sum_{l=1}^{m-2} \epsilon_l t^l, t^n + \sum_{l=1}^{n-2} \mu_l t^l + \sum_{l=n+1}^{c-1} \mu_l t^l \right), \tag{24}$$

where c is the conductor. Of course, $c-1$ is the upper limit for powers of the unfolding, and the highest power may often be smaller than n. In our example of the swallowtail singularity germ (t^3, t^4) (denoted E_6 in the more formal classification of Appendix B), choosing $i=0$ and $j=1$ in (23) yields $1+im+jn=5$, which eliminates 5 from the set of gaps G, and the remaining gaps are 1 and 2. In conclusion, the miniversal unfolding is

$$(t^3 + \epsilon_1 t, t^4 + \mu_1 t + \mu_2 t^2),$$

and thus $\mathrm{cod}(f) = 3$.

This concludes the construction of the unfolding of monomial germs. As for the codimension, a more detailed theory permits to derive the general formula [31]

$$\mathrm{cod}(f) = (m-1)(n-1)/2, \tag{25}$$

which indeed yields cod = 3 for (t^3, t^4). Another theorem which characterizes the codimension geometrically, and is valid for monomial germs only, states that the codimension equals the maximum number of double points (intersections) which are generated with the unfolding of the singularity. This clearly is the case for the cusp singularity shown in Fig. 3, whose unfolding $(t^2, t^3 + \mu_1 t)$ has a self-intersection for $\mu_1 < 0$. In Fig. 8 we show the unfolding of the E_6 singularity germ (t^3, t^4), which exhibits 3 crossings. Another characterization of the number of crossings states that it equals the number of gaps in the semigroup [28, 30, 31].

Now we consider the unfolding of the A_4 germ (t^2, t^5), to be discussed in more detail below. The semigroup is $S(f) = \{2, 4, 5, \dots\}$, with gaps $G = \{1, 3\}$. Using a tangent space transformation, all ϵ_l can be eliminated from $x(t)$; in addition, the w_y tangent space (22)

gives $n - m + im + jn > 3$, and thus does not yield any additional elimination. Thus the miniversal unfolding is

$$(t^2, t^5 + \mu_1 t + \mu_3 t^3), \tag{26}$$

with cod $= (2-1)(5-1)/2 = 2$, which also equals the number of gaps.

To show that the unfolding may contain powers greater than n, we consider the germ

$$(t^m, t^n) \equiv \left(t^4, t^5\right).$$

Eliminating all terms of the semigroup, the unfolding is

$$\left(t^4 + \epsilon_1 t + \epsilon_2 t^2, t^5 + \mu_1 t + \mu_2 t^2 + \mu_3 t^3 + \mu_6 t^6 + \mu_7 t^7 + \mu_{11} t^{11}\right).$$

However, using the additional powers (23), where $n - m = 1$, we can also eliminate the powers $6 = 5 + 1$ and $11 = 10 + 1$, but not 7, since $6 \in G$. Hence the miniversal unfolding finally becomes

$$\left(t^4 + \epsilon_1 t + \epsilon_2 t^2, t^5 + \mu_1 t + \mu_2 t^2 + \mu_3 t^3 + \mu_7 t^7\right) \tag{27}$$

and cod $= 6$, which agrees with (25). Here t^7 is a power greater than that of the germ t^n, corresponding to the second sum in the y-component of (24).

C. A second monomial

We now consider the germ

$$(t^m, t^n \pm t^p), \tag{28}$$

with $p > n$. Clearly, the prefactors can still be normalized to unity, rescaling both x, y and t; however if $n - p$ is even, germs with two different signs are not equivalent. Indeed, the germ with a + sign corresponds to a curve without a self-crossing, the other germ crosses itself. Two different cases need to be considered. In the first case, hcf$(m, n) = 1$, in which case the Puiseux exponents are the same as in the monomial case, and the genus is once more $g = 1$. The exponent p must be such that (28) is not equivalent to the corresponding monomial germ (17); in this case p is called the Zariski exponent. Apart from the Puiseux exponents, the Zariski exponent (or Zariski invariant) is an *invariant* of the representation (28) under all possible transformations.

The Zariski exponent cannot be in the semigroup $S_f =< m, n >$, otherwise a left transformation of the type

$$\tilde{x} = x, \quad \tilde{y} = y - x^i y^j,$$

analogous to (19), would be able to eliminate the extra term t^p. However, there exists a larger class of transformations capable of eliminating t^p, as the example of the germ

$$\left(t^3, t^4 + t^5\right) \tag{29}$$

shows. As we have seen above, t^5 lies in the set of gaps $G = \{1, 2, 5\}$ of the semigroup. However, a more general transformation permits to eliminate t^5: first, we consider the left transformation

$$\tilde{x} = x + \alpha y, \quad \tilde{y} = y,$$

followed by the right transformation

$$\tilde{t}^3 = t^3 + \alpha(t^4 + t^5),$$

where α is a real parameter to be determined. Both transformations are invertible, and from the second one obtains $t = \tilde{t} - \alpha\tilde{t}^2/3$, so that

$$\tilde{y} = t^4 + t^5 = \tilde{t}^4 + \left(1 - \frac{4\alpha}{3}\right)\tilde{t}^5 + O(\tilde{t}^6).$$

Thus if we choose $\alpha = 3/4$, the term of order $\tilde{t}^5$ vanishes, and (29) transforms to

$$\left(\tilde{t}^3, \tilde{t}^4 + O(\tilde{t}^6)\right).$$

Since the terms of order $\tilde{t}^6$ can be eliminated successively, this implies that (29) is indeed equivalent to (t^3, t^4).

In a more systematic fashion, one can show [32–36] that t^p *cannot* be eliminated if and only if p can be represented in the form

$$p = i_1 n - i_0 m, \quad 2 \leq i_0, \quad 2 \leq i_1 < n - 1, \tag{30}$$

and both $p, p+m \in G$. In the example (29), T^5 is not a Zariski exponent since $5+m = 9 \notin G$, and it thus can be eliminated, as we have shown. On the other hand, t^7 in

$$\left(t^4, t^5 + t^7\right) \tag{31}$$

is a Zariski exponent, since the gaps are $G = \{1, 2, 3, 6, 7, 11\}$, so that $7, 7 + 4 \in G$. In addition, 7 can be represented in the form (30) with $i_1 = 3$ and $i_0 = 2$, which satisfies all the conditions. Thus (31) is not equivalent to (t^4, t^5), and represents a new germ.

The second case which arises for germs of the form (28) is that of $hcf(m, n) > 1$, but in which case we must have $hcf(m, n, p) = 1$, otherwise the germ would be trivially reducible by substituting the common factor of all the exponents. The Puiseux exponents are now $\beta_0 = m$, $\beta_1 = n$, and $\beta_2 = p$, and the genus of the germ is 2. Since the Puiseux exponents are invariants, in this case (28) is not reducible to any other (monomial) germ. This completes the classification of germs of the form (28).

1. Unfoldings for two monomials

The unfolding of germs of the type (28) clearly demonstrates the difference between germs with two terms and monomial germs. Essentially, the extra power means that more unfolding terms can be eliminated, and so the codimension decreases. To find the unfolding for more complicated germ, we follow the same procedure as for the monomial germ in constructing the tangent directions (21).

To illustrate that, we consider the germ $(t^4, t^5 + t^7)$. From the condition $w_x = 0$ one finds (omitting the sum and a non-essential prefactor)

$$\epsilon(t) = -a_{ij} t^{4i-3} (t^5 + t^7)^j,$$

so that w_y is of the form

$$w_y = \left[b_{ij} - (5t + 7t^3) a_{ij} \right] t^{4i} (t^5 + t^7)^j.$$

By choosing b_{ij}, we can eliminate all powers in the semigroups $< 4, 5 >= (0, 4, 5, 8, 9, 10, 12 \dots)$ and $< 4, 7 >= (0, 4, 7, 8, 11, 12 \dots)$, and $< 5, 7 >= (0, 5, 7, 10, 14, \dots)$, which leaves t^6 among the powers greater than 4 which cannot be eliminated. However, using the leading power in front of a_{ij}, we can generate terms of the form $5t \times t^{4i} t^{5j}$ which produces t^6 if we choose $i = 0$ and $j = 1$. Thus the unfolding is

$$\left(t^4 + \epsilon_1 t + \epsilon_2 t^2, t^5 + t^7 + \mu_1 t + \mu_2 t^2 + \mu_3 t^3 \right), \tag{32}$$

to be compared to that of the corresponding monomial germ (27). The codimension is only 5 instead of 6, since the extra power can be used to eliminate the unfolding term t^7. The

number of crossings the unfolding (32) produces remains to be 6, since it only depends on the number of gaps, which is the same in both cases. The unfolding of genus-two germs (28), for which $\mathrm{hcf}(m,n) > 1$, is analyzed along similar lines. For example, the unfolding of $(t^4, t^6 + t^7)$ is

$$\left(t^4 + \epsilon_1 t + \epsilon_2 t^2, t^6 + t^7 + \mu_1 t + \mu_2 t^2 + \mu_3 t^3 + \mu_5 t^5\right),$$

and so the codimension is 6.

IV. BIFURCATIONS AND SCALING

The unfolding of a singularity describes the local behavior near the point of highest symmetry. In particular, we focus on the self-similar properties of families of unfoldings, which occur near bifurcation points. As we have seen, the total number of parameters is determined by the codimension, calculated from (25) in the most common case of monomial germs. A self-similar description reduces the number of parameters, and describes the geometry in terms of universal scaling functions. The behavior of the curve under a rescaling is determined by a set of characteristic scaling exponents. The geometry is characterized to a significant extend by the number of double points (self-crossings) δ_f, given by (A6).

At the bifurcation center, where all the unfolding parameters are zero, the scaling of the singularity is determined by the leading monomial terms t^m and t^n; the structure of the unfolding determines the shape of the curve or similarity function. In addition, there are other places in parameter space where bifurcations occur, determined by the condition that the curve becomes singular. In the notation of Section II, for a plane curve we have $n = 1$ and $p = 2$, so the condition for a curve to be singular reduces to $\dot{x} = \dot{y} = 0$. For example, consider the unfolding of the A_4 singularity (in the classification of Appendix B):

$$F : x = \frac{t^2}{2}, \quad y = \frac{t^5}{5} + \frac{\mu_3}{3} t^3 + \mu_1 t, \tag{33}$$

so the codimension is two. The complete diagram of unfoldings is illustrated in Fig. 5, to be derived in more detail below. From $\dot{x} = 0$ we have $t = 0$, so that $\dot{y} = 0$ leads to $\mu_1 = 0$, while μ_3 is arbitrary. The line of critical points $\mu_1 = 0$ corresponds to the formation of a 3/2 cusp at the tip of the curve. We will come back to a more detailed analysis below.

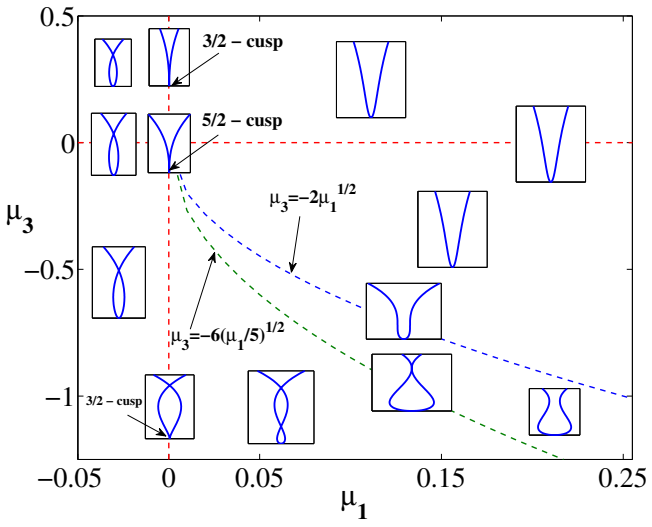

FIG. 5. Bifurcation diagram of the unfolding of the A_4 singularity (33). The bifurcation center $\mu_1 = \mu_2 = 0$ corresponds to a 5/2-cusp; for the critical case $\mu_1 = 0$ a 3/2-cusp singularity is formed at the tip, with the curve self-intersecting for $\mu_3 > 0$. In the remaining four quadrants, for $\mu_3 \propto |\mu_1|^{1/2}$ the curve forms a sequence of self-similar shapes. Along the line $\mu_3 = -6\sqrt{\mu_1/5}$, $(\mu_1 > 0)$, this sequence forms a single bubble, while for $\mu_3 = -2\sqrt{\mu_1}$, $(\mu_1 > 0)$, a channel with vertical tangents is formed. For $\mu_3 < -6\sqrt{\mu_1/5}$ the curve has two double points, for $\mu_1 < 0$ a single double point.

A. Scaling of curves near bifurcations.

We begin with an analysis of monomial germs, whose unfoldings have the structure given by (18). In the miniversal unfolding, the two sums contain a total of $(m-1)(n-1)/2$ terms, corresponding to the codimension. The sum in the x-component runs from $l = 1$ to $l = m-2$, the sum in y-component depends on the gaps of the semigroup, and thus can run up $c-1$ only, where c is the conductor.

If we take ϵ as a typical scale of the curve in the x-direction, we define $t = \epsilon^{1/m}\sigma$, where σ parameterizes the rescaled profile. To determine the scaling exponent α of $y = \epsilon^{\alpha} Y(\sigma)$, we impose a *matching condition* to the far-field behavior [5]. Namely, we impose that far away from the center, the curve is independent of ϵ (of the size of the singular feature), thus ensuring that it can be matched to an outer solution which is independent of ϵ. For

this to make sense, all the powers t^l with $l > n$ in (24) must vanish, because they would dominate the leading power of the germ. Thus we can assume that the far-field behavior is $x = t^m, y = t^n$, and obtain $y = \epsilon^{\alpha - n/m} x$. For this to be independent of ϵ we have $\alpha = n/m$, so that the self-similar form of the curve is

$$(x, y) = \big(\epsilon X(\sigma), \epsilon^{n/m} Y(\sigma)\big) \equiv (\epsilon X, \epsilon^{\alpha} Y)\,; \tag{34}$$

any rational scaling exponent α may be realized by a proper choice of the monomial germ.

To make (34) self-similar, we need X, Y to be independent of ϵ, which is achieved by the scaling

$$\gamma_l \equiv \epsilon_l \epsilon^{(l-m)/m}, \quad \lambda_l \equiv \mu_l \epsilon^{(l-n)/m}.$$

Once more we see that this makes sense only if $l < n$, since otherwise $\mu_l \to \infty$ as $\epsilon \to 0$, which would be inconsistent with the assumption that the unfolding is an infinitesimal perturbation to the germ. Thus we have to put all perturbations with $l > n$ to zero, and the rescaled version of the unfolding becomes:

$$(X, Y) = \left(\sigma^m + \sum_{l=1}^{m-2} \gamma_l \sigma^l, \sigma^n + \sum_{l=1}^{n-2} \lambda_l \sigma^l \right). \tag{35}$$

This defines a family of similarity functions, whose shape depends on the values of the parameters $\gamma_l \ldots, \lambda_l \ldots$. With a proper choice of the parameter ϵ, we can normalize one of the parameters to ± 1, and hence the family of similarity functions is at most $\mathrm{cod}(f) - 1$-dimensional, for each of the two possible signs. Normally one will also require the similarity function to be a smooth curve, so that the singular behavior is captured by the limit $\epsilon \to 0$ alone [5].

The simplest case is the cusp singularity, which results from the smooth deformation of a one-to-one curve (Fig. 6, left) until it self-intersects (right). At the bifurcation point between these two states a cusp is formed. The family of maps which describes this phenomenon is given by the unfolding:

$$x = \frac{t^2}{2}, \quad y = \frac{t^3}{3} + \mu_1 t, \tag{36}$$

determined by a single control parameter μ_1. According to the above, (36) can be written

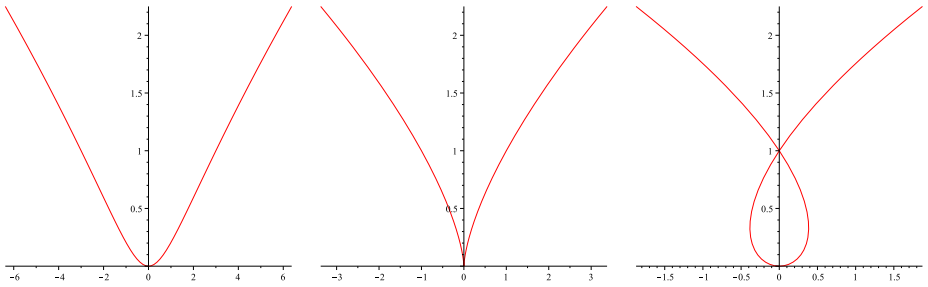

(a) (b) (c)

FIG. 6. The cusp similarity function (37) for $s = 1$, $s = 0$, and $s = -1$, from left to right.

in self-similar form as

$$x = \epsilon X, \quad y = \epsilon^{3/2} Y,$$
$$X = \frac{\sigma^2}{2}, \quad Y = \frac{\sigma^3}{3} + s\sigma, \tag{37}$$

where $\epsilon = |\mu_1|$ and $s = \pm 1$ or vanishes, see Fig. 6. The singular points are given by $X' = \sigma = 0$, $Y' = \sigma^2 + s = 0$, and so $s = 0$ is the bifurcation set, and $\sigma = 0$ corresponds to a singular cusp point, where the curve has a $3/2$ singularity. The cases $s = \pm 1$ describe smooth similarity functions without and with self-intersection, respectively. The singular case $s = 0$ re-emerges as the outer limit $\sigma \to \pm\infty$ of the regular scaling functions $s = \pm 1$.

Another interesting topological feature is one where instead of self-intersecting, the two sides of the curve just touch to form a "bubble", as the limiting case between zero and two intersections, see Fig. 7. The lowest order singularity to realize that is the A_4 singularity, whose unfolding is (26). Following the above prescription, the characteristic scaling exponent is $\alpha = 5/2$, and the scaling functions are

$$X = \frac{\sigma^2}{2}, \quad Y = \sigma\left(\frac{\sigma^4}{5} + \frac{\lambda_3}{3}\sigma^2 + s\right), \tag{38}$$

where $s \in \{0, \pm 1\}$, and which are shown in Fig. 7, where s has the prescribed values, and λ_3 is allowed to vary continuously. Once more $X' = Y' = 0$ yields $\sigma = 0$ as the singular point, and $s = 0$ corresponds to a line of bifurcation points (λ_3 arbitrary). For $\lambda_3 \neq 0$, the tip of the curve has a $3/2$ cusp singularity, while the far-field behavior has of course a $5/2$ power law. The case $\lambda_3 = 0$ is the bifurcation center, for which the curve is a pure $5/2$ cusp. The cases $s = \pm 1$ describe smooth similarity functions, but whose outer limit $\sigma \to \pm\infty$

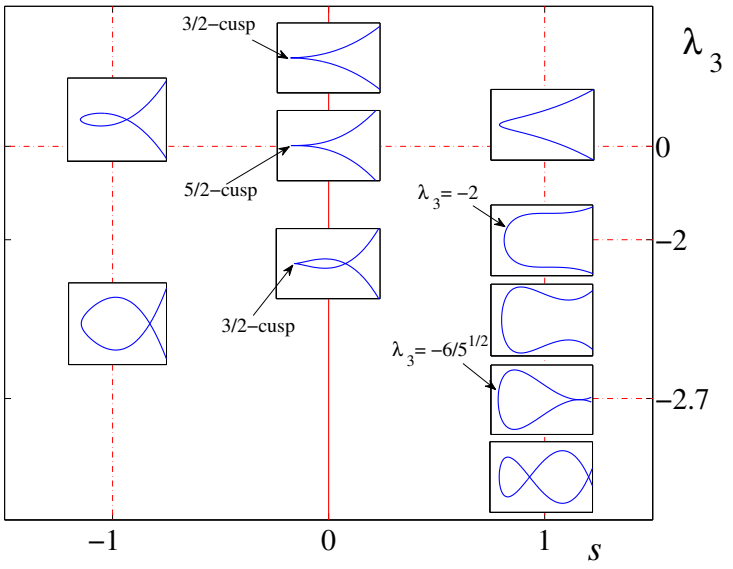

FIG. 7. The bifurcation diagram of the unfolding of A_4 singularity in its scaled form (38).

once more corresponds to the singular case. In the diagram of Fig. 5, they lie along curves $\mu_3 \propto |\mu_1|^{1/2}$.

If $s = -1$, all similarity functions are simple loops with a single self-intersection. For $s = 1$, (38) undergoes a transition from no intersections to two intersection points, which on account of $\mathrm{cod}(f) = 2$ is the maximum number. The critical case of a bubble that forms near the tip is determined by the conditions $Y = Y' = 0$, which leads to the simultaneous system of equations

$$\sigma^4 + \frac{5\lambda_3}{3}\sigma^2 = -5, \quad \sigma^4 + \lambda_3\sigma^2 = -1,$$

having factored out the zero at $\sigma = 0$. The solution is $\lambda_3 = -6/\sqrt{5}$, while the touch point occurs at $\sigma = \pm 5^{1/4}$. Thus the case of a bubble being enclosed is described by the universal similarity function

$$(X, Y) = \left(\frac{\sigma^2}{2}, \frac{\sigma}{5}\left(\sigma^2 - \sqrt{5}\right)^2 \right), \tag{39}$$

and if the height of the bubble scales like ϵ, its width is predicted to scale like $\epsilon^{5/2}$. In a practical situation, when observing the enclosure of a bubble on successively smaller scales, the generic prediction is that the bubble's shape is described by (39), and its size ratio scales like $\epsilon^{5/2}$. Another critical case is the formation of a channel with parallel sides near the tip, characterized by the equations $Y' = Y'' = 0$. Proceeding as before, this corresponds to the

parameter $\lambda_3 = -2$ and $\sigma = \pm 1$. Thus the universal profile for such a channel is

$$(X, Y) = \left(\frac{\sigma^2}{2}, \frac{\sigma}{5} \left(\sigma^4 - \frac{10}{3}\sigma^2 + 5 \right) \right), \tag{40}$$

and the shape is one of those shown in Fig. 7.

Of course, the universal bubble shape (39) is only the lowest order of an infinite hierarchy of possible shapes. On account of symmetry, the similarity function is expected to be of the form

$$(X, Y) = \left(\sigma^2, \sigma f(\sigma^2) \right),$$

with $f(x) = (x - a)^2$ in the simplest case. For example, the choice $f(x) = (x - a)^2(x + 1)$ would lead to a differently shaped bubble, whose width would scale like $\epsilon^{7/2}$. However, the occurrence of such a bubble would be a non-generic situation. However, a higher order singularity could also describe more complex geometries, such as a sequence of n bubbles, which would be achieved by $f(x) = \prod_i (x - x_i)^2$, such that the similarity function is

$$(X, Y) = \left(\sigma^2, \sigma \prod_{i=1}^{n} (\sigma^2 - \sigma_i^2)^2 \right). \tag{41}$$

The size would scale like $\epsilon^{(4n+1)/2}$ in this case.

The unfolding of the E_6-singularity germ:

$$x = \frac{t^3}{3} + \epsilon_1 t, \quad y = \frac{t^4}{4} + \frac{\mu_2}{2} t^2 + \mu_1 t \tag{42}$$

describes among others the "swallowtail" shape which appears in the formation of caustics of wave fronts, to be discussed in much more detail in Sec. V B, see Fig. 9 below. The scaling form of (42) is

$$\begin{aligned} x &= \epsilon X, \quad y = \epsilon^{4/3} Y, \\ X &= \frac{\sigma^3}{3} + s\sigma, \quad Y = \frac{\sigma^4}{4} + \frac{\lambda_2}{2}\sigma^2 + \lambda_1 \sigma. \end{aligned} \tag{43}$$

One only needs to consider $\lambda_1 > 0$, since the transformation $\lambda_1 \to -\lambda_1$, $\sigma \to -\sigma$ only changes the sign of X, so that on obtains a mirror image. To understand the different types of similarity solutions, it is best to find the bifurcation points, defined by $X' = Y' = 0$. If $s = 0$, it follows that $\sigma = 0$ and thus $\lambda_1 = 0$. As seen on the top right of Fig. 8, there is a

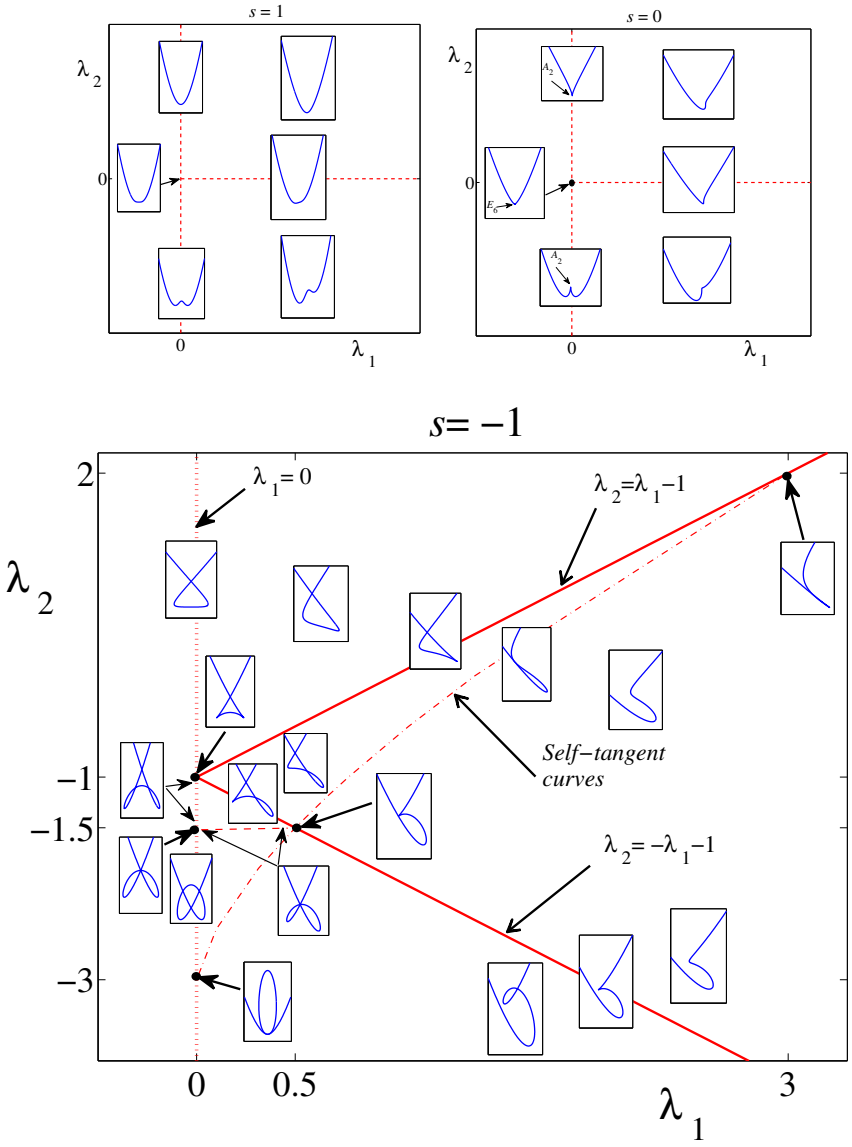

FIG. 8. Bifurcation curves for the E_6 singularity, as represented in its scaled form (44). On top, unfolding for $s = 1$ and $s = 0$, at the bottom, the bifurcation diagram for $s = -1$ [9].

3/2 cusp singularity at the center of the curve. Clearly, if $s = 1$, there is no solution with $X' = 0$, and (X, Y) is a smooth, non-intersecting curve (cf. Fig. 8, top left).

The most interesting case arises for $s = -1$, such that critical points are at $\sigma = \pm 1$. Inserting this into $Y' = 0$, one finds two lines of critical points, $1 + \lambda_2 \pm \lambda_1 = 0$, which are shown as solid lines at the bottom of Fig. 8), which separate the phase diagram into four distinct regions. Only the right hand side $\lambda_1 > 0$ of the phase diagram is shown, as the left hand side is the same by symmetry. To understand what happens on the critical lines we

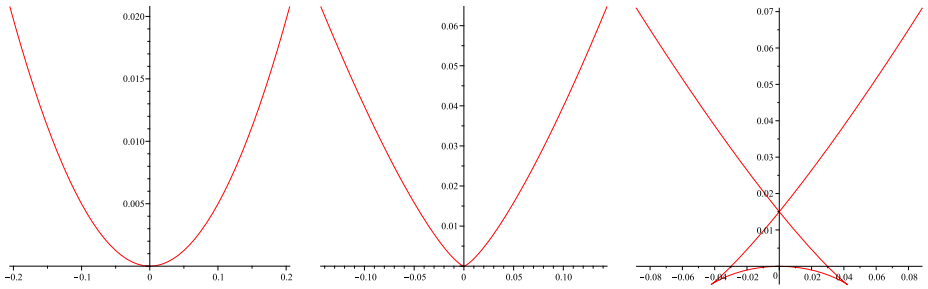

(a) (b) (c)

FIG. 9. The swallowtail similarity function (45) for $s = 1$, $s = 0$, and $s = -1$, from left to right.

put $\lambda_2 = -1 \mp \lambda_1 + \epsilon$ and $\sigma = \pm 1 + \delta$, and expand to third order in δ:

$$(X, Y) = \left(\mp\frac{2}{3}, -\frac{1}{4} + \frac{\epsilon \pm \lambda_1}{2}\right) + \left(\pm\delta^2 + \frac{\delta^3}{3}, \pm\epsilon\delta + \left(1 + \frac{\epsilon \mp \lambda_1}{2}\right)\delta^2 \pm \delta^3\right).$$

Using the transformation

$$(\tilde{X}, \tilde{Y}) = \left(X, Y \mp \left(1 + \frac{\epsilon \mp \lambda_1}{2}\right) X\right) = \tag{44}$$
$$\left(\mp\frac{5}{12} + \frac{5\epsilon \pm \lambda_1}{6}\right) + \left(\pm\delta^2 + O(\delta^3), \pm\epsilon\delta + \left(\pm\frac{2}{3} + \frac{\lambda_1 \mp \epsilon}{6}\right)\delta^3\right),$$

this transforms into a cusp (36), with ϵ being the unfolding parameter.

Thus at points along the critical lines ($\epsilon = 0$), lower order cusp singularities are formed locally. At the point $\lambda_1 = 0$, $\lambda_2 = -1$ where both lines cross, the figure has two cusp points, with similarity function

$$X = \frac{\sigma^3}{3} + s\sigma, \quad Y = \frac{\sigma^4}{4} + s\frac{\sigma^2}{2}, \tag{45}$$

and $s = -1$, which is often referred to as the swallowtail shape in catastrophe theory [17]. In Fig. 9 we show the cases $s = 1$, $s = 0$ together with the swallowtail $s = -1$. The swallowtail sits at the center of the bifurcation diagram in Fig. 8; it has the shape of a wave front near a caustic, and plays an equally important role for the formation of shocks (cf. Sec. V C).

As one moves away from the critical line ($\epsilon \neq 0$ in (45)), the local cusp singularity unfolds, as seen in Fig. 6. For example, moving to the right of the lower bifurcation line (upper sign in (45) and $\epsilon > 0$), the cusp opens. Moving to the left of the same bifurcation line ($\epsilon < 0$), the curve self-intersects to form a loop.

To give a more complete description of the possible topologies, a few more lines have been added to Fig. 8, although they do not correspond to bifurcations; along $\lambda_1 = 0$ (dotted line),

the curve is symmetric. Along the dot-dashed line, the curve is tangent to itself; across it, self-intersecting loops are opened. This allows one to go continuously from the upper bifurcation line to the lower bifurcation line via non-intersecting curves. However, only the end points of this curve are known analytically, the line in between has to be calculated numerically.

Finally, the dashed line marks curves with triple points (three points of the curve coinciding), and is given by $\lambda_2 = -3/2$ and $|\lambda_1| \leq 1/2$. The triple points occur on the line $Y = 0$, and thus are determined by the equation

$$\sigma^3 - 3\sigma + 4\lambda_1 = 0;$$

along the dashed line, the discriminant is negative, so there are three real roots. Solutions are given by

$$\sigma = 2\cos\left[\lambda - \frac{2\pi k}{3}\right], \quad k = 1, 2, 3,$$

where $\lambda = \arccos(-2\lambda_1)/3$. A direct calculation shows that $X = \sigma^3/3 - \sigma$ is the same for all three solutions, which thus represent a triple point.

The swallowtail shape (45) can be combined with the idea of a bubble of vanishing size to produce another universal shape. Instead of self-intersecting (cf. Fig. 9, right), the two sides just touch to inclose a bubble, see Fig. 10. This means there are critical points at some $\sigma = \pm 1$, which we can normalize to unity. In addition, the Y-component has minima at another value $\sigma = \pm\sigma_0$, leading to the ansatz

$$(X', Y') = \left(\sigma(\sigma^2 - 1), (\sigma^2 - 1)(\sigma^2 - \sigma_0^2\right).$$

Integrating, we demand that $Y(\sigma_0) = 0$, with solution $\sigma_0 = \sqrt{5}$, and we obtain the similarity function

$$(X, Y) = \left(\frac{\sigma^2}{4}\left(\sigma^2 - 2\right), \frac{\sigma}{5}\left(\sigma^4 - 10\sigma^2 + 25\right)\right), \tag{46}$$

shown in Fig. 10; the width of this bubble scales like $\epsilon^{5/4}$.

The profile (46) appears as a particular case in the unfolding of the singularity germ (t^4, t^5), whose complete unfolding is (27). To be consistent with the matching condition, we have to put $\mu_7 = 0$, but which would still leave us with a four-dimensional parameter space. Thus we restrict ourselves to symmetric shapes, with x an even function and y an odd function, i.e. $\epsilon_1 = \mu_2 = 0$. The similarity function becomes

$$(X, Y) = \left(\frac{\sigma^4}{4} + \frac{s\sigma^2}{2}, \frac{\sigma^5}{5} + \frac{\lambda_3}{3}\sigma^3 + \lambda_1\sigma\right), \tag{47}$$

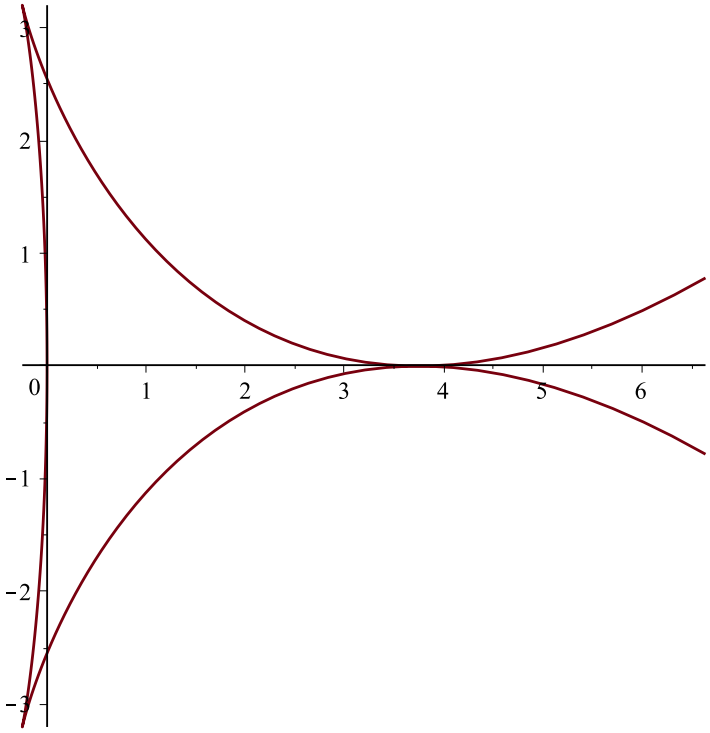

FIG. 10. A bubble in the form of a swallowtail, as described by the similarity function (46).

with the bifurcation diagrams for the three different cases $s = 0, 1, -1$ being shown in Fig. 11. For any value of s, singular points are given by $\sigma = \lambda_1 = 0$, λ_3 arbitrary. In the case $s = -1$, there is an additional pair of singular points $\sigma = \pm 1$, $\lambda_1 = -1 - \lambda_3$, shown as the thick solid line.

For negative values of λ_1, all curves have at least one self-intersection. Turning to positive values of λ_1, there is a self-tangent point on the line of symmetry if $Y = Y' = 0$ is satisfied, which leads to $\sigma^2 = -6\lambda_1/\lambda_3$, which means we must have $\lambda_3 < 0$. In that case, self-tangent curves lie along the line $\lambda_1 = 5\lambda_3^2/36$ shown in all three figures. Thus in the second quadrant of all three diagrams, below this line the corresponding curves have at least two self-intersection points. A horizontal turning point is given by $Y' = Y'' = 0$, which leads to $\sigma^2 = -\lambda_3/2$ and thus $\lambda_3 < 0$, as well as $\lambda_1 = \lambda_3^2/4$, which is also shown in Fig 11. In between these two parabolas, curves have two horizontal tangents. An additional feature of the case $s = -1$ is the straight bifurcation line $\lambda_1 = -1 - \lambda_3$ along which curves have a pair of cusp points. At the intersection with the self-tangent curve one finds the "bubble" shown in Fig. 10.

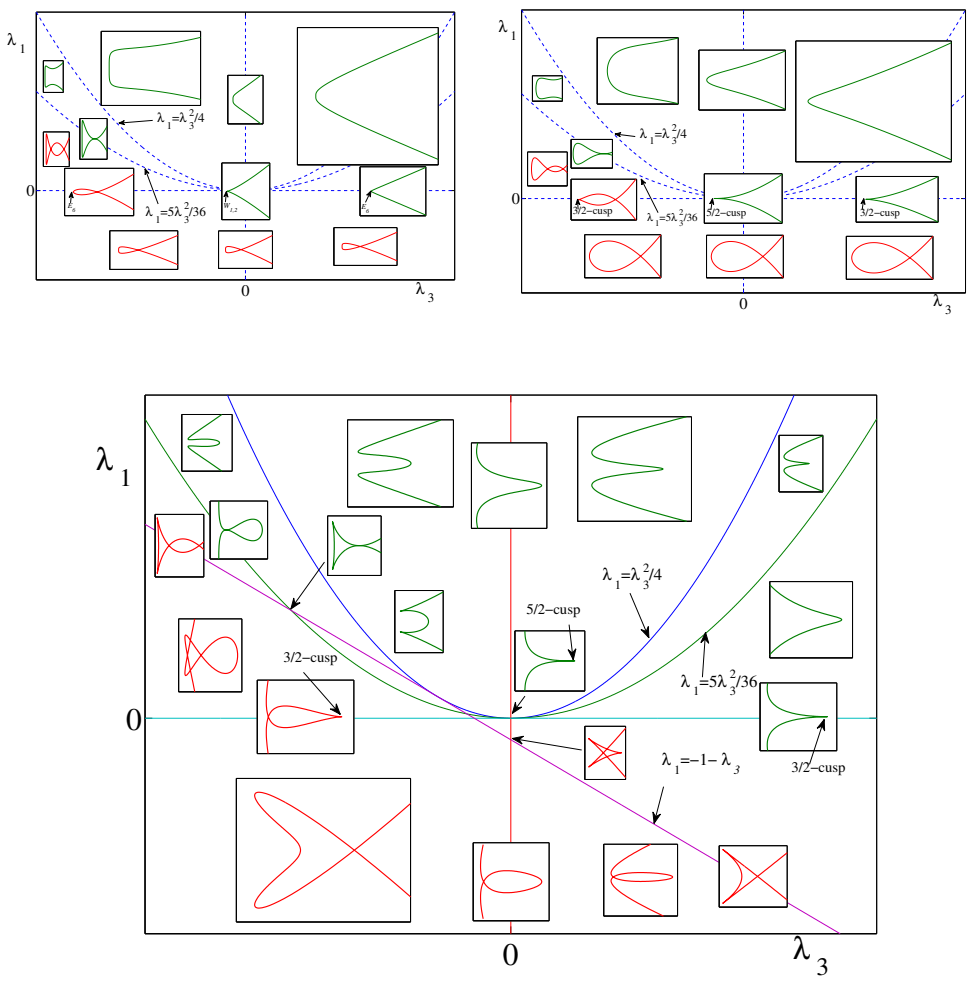

FIG. 11. Bifurcation curves for the $W_{1,2}$ singularity with additional symmetry, see (47). On top, unfolding for $s = 1$ and $s = 0$, at the bottom, the bifurcation diagram for $s = -1$.

B. Scaling with two monomials

We have seen above that monomial germs describe a family of similarity solutions whose scaling exponent is fixed by the leading powers m and n. In the case of two monomials, $(t^m, t^n \pm t^p)$ with $p > n$, the power law behavior will be different depending on whether one is considering the limit $t \to 0$ or $t \to \infty$. In that sense, these germs describe the *crossover* between two different scaling behaviors on the small and large scale, respectively.

To be more precise, the scaling

$$(x, y) = (\epsilon X, \epsilon^{n/m} Y) \tag{48}$$

leads to the similarity form

$$(X, Y) = \left(\sigma^m + \sum_l \gamma_l \sigma^l, \sigma^n \pm \epsilon^{(p-n)/m} \sigma^p + \sum_l \lambda_l \sigma^l \right).$$

Thus in the limit $\epsilon \to 0$, the second monomial drops out and scaling is described by (35). If on the other hand $\Gamma \to \infty$, the leading order behavior would be $(x, y) = (\Gamma X, \Gamma^{p/m} Y)$, the monomial σ^n becoming subdominant.

V. APPLICATIONS

Applications to physical problems clearly hinge on whether we can guarantee the existence of a smooth mapping, whose singularities we would like to analyze. A simple example was giving in the introduction, where we analyzed the pinch-off of a cavity inside a viscous fluid, whose singularities were determined by the singular points of a smooth mapping $\mathbb{R} \to \mathbb{R}$. However, we saw that the "inverse" problem of a viscous drop pinching off in air was of a different nature [5]. In that case one of the scaling exponents is an irrational number, while scaling found within singularity theory is of the rational type. In addition, in Sections V G 1 and V I we provide explicit examples of problems which are described by a piecewise smooth mapping, but different parts of the solution lie on different branches of the function. The singularity appears exactly at the boundary between two branches, making singularity theory inapplicable. As a result, the observed singularities are of a type not included in the classification of singularity theory.

If the physical problem is described by a smooth mapping (which is often found by a (complex) mapping technique [37]), the function will depend on time or on an arbitrary number of physical control parameters, which we will point out in specific examples below. Singularity theory then allows us to classify the possible singularities that may occur; however, no predictions can in general be made about whether a given singularity *will* occur, since this depends on the global nature of the mapping, and the values the control parameters may attain. Also, the unfolding may not be the most general one, but be restricted by symmetries of the problem. A closer analysis of the specific mapping may often reveal of which type the singularity may be and how the unfolding may look like.

In addition, it lies in the local nature of singularity theory that it cannot predict actual values of parameters where a singularity may occur. The singularity and its unfolding can be

found up to smooth invertible transformations, for example a rotation. Thus the orientation of a particular figure cannot be predicted, and only up to a transformation which changes the scale of the problem. Apart from that, the analysis is very powerful, since it makes predictions without any explicit calculations, merely relying on the existence of a smooth mapping. It also points to relations and similarities between seemingly very different physical problems.

A. The Hamilton-Jacobi equation: Caustics and shock waves

In general, singularities of plane curves involve the analysis of mappings $f : \mathbb{R} \to \mathbb{R}^2$, as we have done above. However, there is a particular sub-class of problems in which curves can be characterized as the critical points of a single, *scalar-valued*, function. This framework, which involves the classification of scalar functions only (called generating functions in this context) is that of catastrophe theory [13, 17]. In it, two different objects, known as Lagrangian and Legendre singularities, are connected through the generating function. A general framework in which these types of singularities arise is that of the Hamilton-Jacobi equation [14, 38], which we will describe now. Two particular physical examples are the eikonal equation, which describes the formation of caustics of an advancing wave front, and the kinematic wave equation, which is the simplest equation exhibiting shocks.

We begin with an action $S(q,t)$, which depends on the generalized coordinate q as well as on time. In the spirit of this review, we consider a single coordinate q, but the same formalism applies to a vector quantity $\mathbf{q}$. We assume that S satisfies the Hamilton-Jacobi equation

$$\frac{\partial S}{\partial t} + H\left(q, \frac{\partial S}{\partial q}, t\right) = 0, \tag{49}$$

with initial condition $S(q,0) = S_0(q)$. In classical mechanics [38], $H(q,p,t)$ is the Hamiltonian of a mechanical system. The PDE problem (49) can be solved as a mechanical (ODE) problem by the method of characteristics. To that end let $p = \dfrac{\partial S}{\partial q}$ be the canonical momentum, and we solve the Hamilton equations

$$\dot{q} = \frac{\partial H}{\partial p}, \quad \dot{p} = -\frac{\partial H}{\partial q} \tag{50}$$

with initial conditions

$$q(0) = q_0, \quad p(0) = \frac{\partial S_0}{\partial q_0}. \tag{51}$$

Then $S(q,t)$ can be recovered by integrating along the characteristics:

$$S(q,t) = S_0(q_0) + \int_\gamma L(q,\dot{q},t)dt, \tag{52}$$

where $L(q,\dot{q},t)$ is the Lagrange function corresponding to the Hamiltonian $H(q,p,t)$. The integral is taken along the curve γ, which is the solution curve obtained from integrating (50), with initial conditions (51). The action (52) is now a solution to the PDE (49) with initial condition $S(q,0) = S_0(q)$ [14].

Instead of specifying the two initial conditions (51) to find γ, one can also specify the initial condition $q_0 = \overline{q}(0)$, as well as the end point $q = \overline{q}(t)$, where we denote the trajectory with an overbar for clarity. In this way we can now write the action

$$S(q,t;q_0) = S_0(q_0) + \int_0^t L(\overline{q}(q,t;q_0), \dot{\overline{q}}(q,t;q_0), t)dt, \tag{53}$$

which at constant q_0 is still a solution to the Hamilton-Jacobi equation (49). However, the second initial condition (51) will in general *not* be satisfied. Now taking the derivative with respect to q_0, integrating by parts and using the fact that the Lagrange equation is satisfied along $\overline{q}$, we find

$$\frac{\partial S}{\partial q_0} = \frac{\partial S_0}{\partial q_0} + \left[\frac{\partial L}{\partial \dot{\overline{q}}}\frac{\partial \overline{q}(q,0;q_0)}{\partial q_0}\right]_{\overline{q}=q_0}^{\overline{q}=q} = \frac{\partial S_0}{\partial q_0} - p(0),$$

since $\dfrac{\partial q}{\partial q_0} = 0$ and $\dfrac{\partial q}{\partial q} = 1$. Thus the true trajectory, which satisfies the initial conditions (51), can be found from the extremal condition

$$\frac{\partial S(q,t;q_0)}{\partial q_0} = 0. \tag{54}$$

Singularities arise because characteristics (or particle paths in mechanical language) cross, and hence the action becomes multivalued; this means that $\partial q/\partial q_0 = 0$. Differentiating (54), we have

$$0 = \frac{d}{dq_0}\frac{\partial S(q,t;q_0)}{\partial q_0} = \frac{\partial^2 S}{\partial q_0^2} + \frac{\partial S}{\partial q}\frac{\partial q}{\partial q_0},$$

and thus in terms of the action, a crossing of trajectories implies

$$\frac{\partial^2 S(q,t;q_0)}{\partial q_0^2} = 0. \tag{55}$$

The set defined by (55) is the *bifurcation set* (13). We see that the action $S(q,t)$ is described implicitly by the critical points (54), noting that instead of q_0 we can use any quantity φ to

parameterize the action; such a variable is called the *state variable*. The *configuration space* is determined by the parameters q and time t.

Following Arnold [39], we can construct the *Legendre manifold* (a smooth curve in (p, q, S)-space) by

$$S = S(q, t, \varphi), \quad \frac{\partial S}{\partial \varphi} = 0, \quad p = \frac{\partial S}{\partial q}. \tag{56}$$

The projection of the manifold onto the (q, S)-plane is called the Legendre map, whose image is determined by the first two equations of (56). This image will in general be singular, namely at points where the condition $\partial q/\partial \varphi = 0$ is met; we will see below that in optics, this set defines a wave front.

On the other hand, the *Lagrange manifold* is defined in the plane (q, p) by

$$\frac{\partial S}{\partial \varphi} = 0, \quad p = \frac{\partial S}{\partial q}. \tag{57}$$

Its projection onto q again has singular points when $\partial q/\partial \varphi = 0$, or in other words when

$$\frac{\partial S}{\partial \varphi} = 0, \quad \frac{\partial^2 S}{\partial \varphi^2} = 0. \tag{58}$$

Projected onto the (q, t) plane, all points which satisfy (58) are known as the *caustic*.

The generic form of the singularity (55) is represented by the germ is $S = \varphi^3$, near which the action becomes

$$S = \varphi^3 - \alpha\varphi. \tag{59}$$

The parameter α can be seen as a function of q and t if the initial condition $S_0(q)$ is held fixed, but may equally well be seen as varying with any number of parameters characterizing the initial condition. The caustic lies at $\alpha = 0$ (where the conditions (58) are satisfied), which is a line in the (q, t)-plane. The solution $S(q, t; \varphi)$ has to satisfy the condition (54), which yields $\alpha = 3\varphi^2$. This means that the action near the caustic line has the form

$$S = -2\varphi^3, \quad \alpha = 3\varphi^2, \tag{60}$$

which is a cusp in the (α, S)-plane. At a given time, α is a smooth function of q, and hence $S(q)$ is also a cusp in the (q, S)-plane.

Since caustics are lines in (q, t)-space, one can ask where they originate, from a smooth initial condition. To answer this, one has to consider the higher-order germ $S = \varphi^4$ with unfolding

$$S = \varphi^4 - \beta\varphi^2 - \alpha\varphi, \tag{61}$$

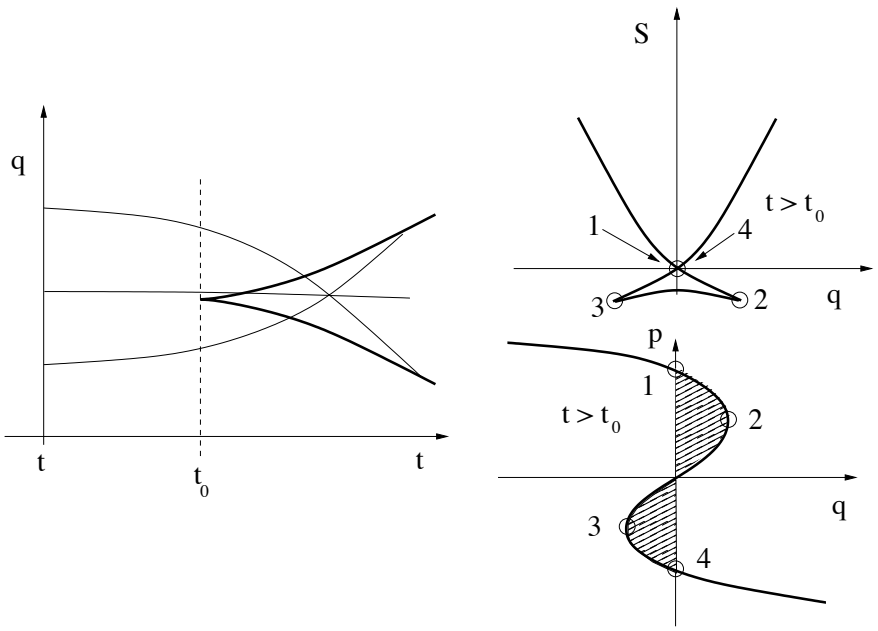

FIG. 12. The generic form of a cusp singularity. On the left, lines are trajectories with the caustic line shown in bold. Inside the caustic, three different trajectories correspond to any given point. On the right, the solution at a time $t > t_0$ after the singularity. The action has the form of a swallowtail, while the momentum forms an s-curve. Taking a path along which S is single-valued corresponds to jumping from the upper branch of the s-curve to the lower branch in such a way that the shaded areas are equal.

where now both α and β are functions of q, t at fixed initial condition. Performing a coordinate transformation such that $\beta = \bar{t} \equiv t - t_0$ and $\alpha = q$, the situation is as shown in Fig. 12, where t_0 is the time where a singularity first occurs. From (58) one has $q = 4\varphi^3 - 2\bar{t}\varphi$ and $\bar{t} = 6\varphi^2$, and thus

$$\bar{t} = 6\varphi^2, \quad q = -8\varphi^3 \tag{62}$$

is the caustic, which has the form of a cusp, as shown on the left-hand side of Fig. 12. Accordingly, this is known as the *cusp catastrophe*. There is no singularity for $t < t_0$, i.e. for $\bar{t} < 0$, which shows that our above identification of the parameters α and β was correct. The action is

$$S = 3\varphi^4 - \bar{t}\varphi^2, \quad q = 4\varphi^3 - 2\bar{t}\varphi, \tag{63}$$

which is the swallowtail function (45) introduced before. It can be seen as the projection of

the Legendre manifold

$$S = 3\varphi^4 - \bar{t}\varphi^2, \quad q = 4\varphi^3 - 2\bar{t}\varphi, \quad p = -\varphi, \tag{64}$$

which is a smooth curve. For $\bar{t} > 0$ is has the form of a swallowtail, shown on the right of Fig. 12. Within the range of q-values inside the cusp on the left, three different values for S are found. This corresponds to three different rays that can reach any point inside the cusp. The momentum $p = \partial S/\partial q = -\varphi$ obeys the cubic equation

$$q = -4p^3 + 2\bar{t}p, \tag{65}$$

which is the Lagrange manifold introduced above. Thus for $\bar{t} < 0$ (before the singularity), p has a unique value as function of q, while after the catastrophe, in the region inside the cusp, there are three different values, as shown on the bottom left of Fig. 12. We have

$$S = \int \frac{\partial S}{\partial q} dq = \int p dq,$$

so following the swallowtail curve along the points 1-4 corresponds to integrating the s-curve of the momentum. Going directly from 1 to 4, without passing through the lower portion of the swallowtail, corresponds to jumping down from 1 to 4 in the s-curve. Since $S(q)$ has a unique value, it follows that the total integral over the s-curve from 1 to 4 must be zero: the area of the two shaded lobes are equal, a construction known as Maxwell's rule.

B. The eikonal equation

As a first example, we choose the propagation of light rays, and the singularities generated by it. As illustrated in Fig. 13, there are three different ways in which to describe the propagation of an optical wavefront. Firstly, the action S satisfies a Hamilton-Jacobi equation, and the wave fronts are recovered by considering lines of constant S. Secondly, the corresponding Hamiltonian system describes the path of a ray, which is perpendicular to the wave front. Knowing the optical path length ℓ of a ray, one can reconstruct the wave front as shown in Fig. 13. The optical path length satisfies the same Hamilton-Jacobi equation as function of either pairs of its arguments. Thirdly, the graph of the wave front $h(x,t)$ satisfies another, slightly different Hamilton-Jacobi equation from the one describing the action.

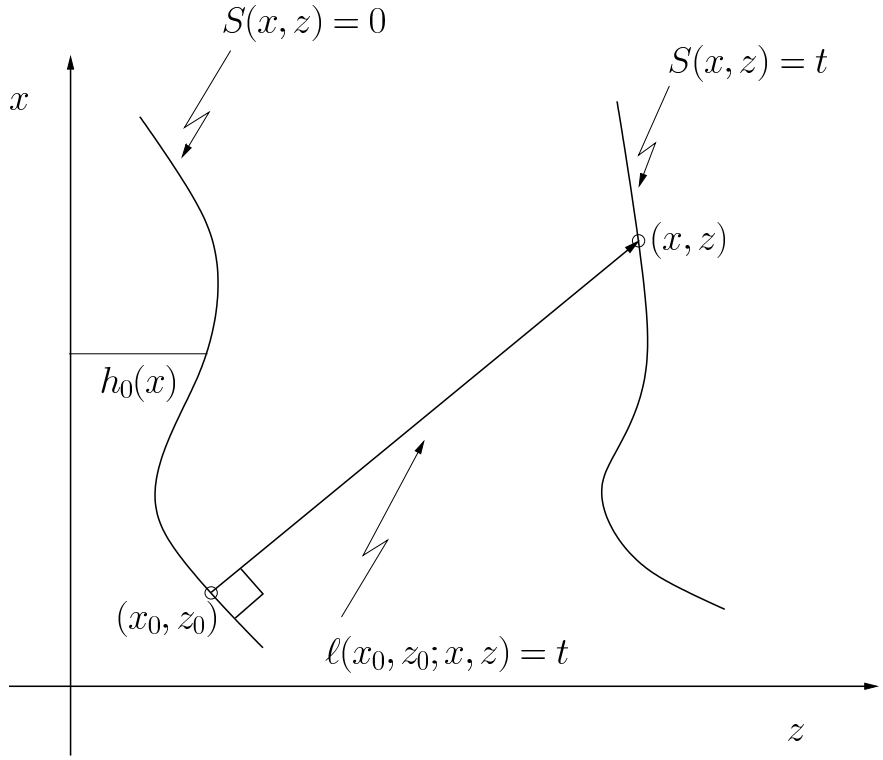

FIG. 13. A wavefront can be described either as the graph of a function $z = h(x,t)$, or as lines of constant value of the action $S(x,z)$. Rays are perpendicular to the wavefronts, and $\ell(x_0,z_0;x,z)$ measures the optical path length between two points.

According to Fermat's principle [40], light rays travel along a path γ such that

$$S = \int_\gamma L dz, \quad L = n(x,z)\sqrt{1+x_z^2} \tag{66}$$

is minimal (with fixed end points). Here the distance z along the optical axis is treated like a time variable in ordinary mechanics, and $n(x,z)$ is the index of refraction. There is no problem in generalizing to 3 spatial dimensions x, y, z.

The canonical momentum is

$$p = \frac{\partial L}{\partial x_z} = n\frac{x_z}{\sqrt{1+x_z^2}}, \tag{67}$$

and so

$$H = px_z - L = -\sqrt{n^2-p^2}. \tag{68}$$

In the free space case $n = 1$ the Hamilton equations (50) are

$$x_z = \frac{p}{\sqrt{1-p^2}}, \quad p_z = 0,$$

so that $p = p_0 = const$, and

$$x = x_0 + \frac{p_0 z}{\sqrt{1 - p_0^2}}, \tag{69}$$

meaning that rays follow a linear path. The Hamilton-Jacobi equation (49) is

$$\left(\frac{\partial S}{\partial z}\right)^2 + \left(\frac{\partial S}{\partial x}\right)^2 = n^2, \tag{70}$$

which in this context is known as the eikonal equation.

Now we define wave fronts as the equipotential lines $S(x, z) = const$ of the action function. We have

$$p = \frac{\partial S}{\partial x}, \quad H = -\frac{\partial S}{\partial z}, \tag{71}$$

and so the normal to a wave front is

$$\mathbf{n} = \frac{\boldsymbol{\nabla} S}{|\boldsymbol{\nabla} S|} = \frac{1}{\sqrt{1 + x_z^2}} \left(x_z, -1\right),$$

where $x(z)$ is the ray path. Thus wave fronts are orthogonal to the direction $(1, x_z)$ of a ray.

Now let $S(x, z)$ be a solution to (49) with initial condition $S(x, z_0) = S_0(x)$. Then according to (52), $S(x, z)$ can be written as

$$S(x, z) = S_0(x_0) + \int_\gamma L dz, \tag{72}$$

where γ is along a light ray from (x_0, z_0) to (x, z). We take the wave front as passing through (x_0, z_0) at $t = 0$, and through (x, z) at t. But this means that

$$\int_\gamma L dz = ct,$$

implying that the evolution of the wave front *in time* is given by

$$S(x, z) = ct, \tag{73}$$

where $S(x, z)$ is any solution of the eikonal equation (70). In future, we will normalize the speed of light c to unity. Given a solution to the spatial problem, the dependence on time can be found using (73).

In the simplest case $n = 1$, rays lie on straight lines (69) and an exact solution to $S(x, z)$ can be found accordingly. However, even in the general case n varying in space, where such a solution is not available, the structure of the first singularity of a wave front must be a cusp catastrophe, and described by (62) and (64), but where $\bar{t}$ is replaced by the "time"

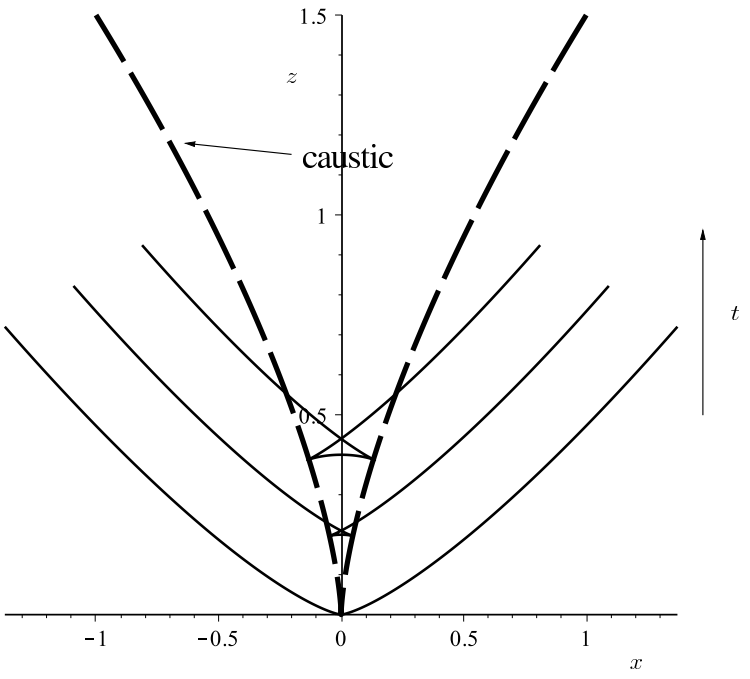

FIG. 14. The cusp catastrophe: wave fronts are swallowtails, the caustic is a cusp, as given by (74) and (75), respectively.

variable z. To understand how the wave front propagates in time and how it lies relative to the caustic surface, we specify that the wave propagates in the z-direction. This means that to leading order, the action looks like $S = z - t$ (or $S = nz - t$ if n is not equal unity). This means that the a line of constant phase propagates at speed $1/n$ in the z-direction. The expression $S = 3\varphi^4 - z\varphi^2$ (cf. (64)) for the action describes its variation around this mean motion. Thus the position of the wave front $z(x)$ as it travels in time is given by

$$z = t + 3\varphi^4 - t\varphi^2, \quad x = 4\varphi^3 - 2t\varphi, \tag{74}$$

where we have used the leading-order result $z \approx t$ on the right-hand side. The singularities of the wave fronts lie on the caustic line

$$z = 6\varphi^2, \quad x = -8\varphi^3, \tag{75}$$

both of which are shown in Fig.14.

To conclude this section, we mention that instead of the Hamilton-Jacobi equation (70) for the path length S, an equivalent Hamilton-Jacobi equation,

$$\frac{\partial h}{\partial t} = \frac{\sqrt{1 + h_x^2}}{n}, \tag{76}$$

can be written for the front $h(x,t)$, as shown in Fig. 13. The two descriptions are connected by the equation $S(x,h(x,t)) = t$. The Hamiltonian is now $H = -\sqrt{1+\overline{p}^2}/n$, where the canonical momentum is $\overline{p} = \partial h/\partial x$. Solving the Hamiltonian equations for the case $n = 1$, one finds a solution to (76) in the form

$$h(x,t) = h_0(x_0) + \frac{t}{\sqrt{1+h_0'^2}}, \quad x = x_0 - \frac{h_0' t}{\sqrt{1+h_0'^2}}, \tag{77}$$

where $h_0(x) = h(x,0)$ is the initial condition.

C. The kinematic wave equation

The shocks that are formed by the kinematic wave equation (or inviscid Burgers' equation)

$$\frac{\partial v}{\partial t} + v v_x = 0 \tag{78}$$

give the same hierarchy of singularities as optical singularities. To see that we write $\phi_x = v$ (which can also be done in higher dimensions), and obtain after integrating

$$\frac{\partial \phi}{\partial t} + \frac{\phi_x^2}{2} = 0, \tag{79}$$

where the constant of integration can be chosen to vanish with an appropriate choice of ϕ. This has the form of a Hamilton-Jacobi equation with action $S \equiv \phi$, and Hamiltonian

$$H(p,x) = \frac{p^2}{2}, \tag{80}$$

where the momentum is $p = \partial\phi/\partial x$. This is the Hamiltonian of a free particle, and clearly the particle trajectories are

$$p = p_0 = const, \quad x = p_0 t + x_0. \tag{81}$$

We can find ϕ using (52), where

$$L = \frac{\dot{x}^2}{2} = \frac{p_0^2}{2} = \frac{(\phi_0')^2}{2}$$

is the Lagrangian. This means that the velocity potential can be written in the form

$$\phi(x,t) = \phi_0(x_0) + \frac{(\phi_0')^2}{2} t, \quad x = \phi_0' t + x_0, \tag{82}$$

and the velocity is

$$v(x,t) = \frac{\partial \phi}{\partial x} = (\phi_0' + \phi_0'' t)\,\frac{\partial x_0}{\partial x} = \phi_0' = v_0(x_0, 0), \tag{83}$$

which is the usual solution by characteristics [41].

The velocity (momentum) as function of x is

$$v = p = \frac{\partial \phi}{\partial x_0} = -x_0, \quad x = 3x_0^3 - \bar{t}x_0, \tag{84}$$

which is shown on the left of Fig. 15. For $\bar{t} < 0$ the solution is regular, but shows a wave which steepens as $\bar{t} = 0$ is approached. For $\bar{t} > 0$ the velocity has the form of an s-curve, and thus can no longer be interpreted as a classical solution of (78). The cusp

$$x = -8x_0^3, \quad \bar{t} = 6x_0^2$$

delineates the region where there are three different v-values to one x-value, so there are three characteristics coexisting. Inside of this region one needs to decide which part of the graph corresponds to a physically realizable solution, as we will do now.

Maxwell's rule The s-shaped velocity profile (84) is unphysical as a solution to the kinetic wave equation (78), in that the profile becomes multivalued. Instead, a shock (i.e. a jump in the velocity) needs to be inserted in order for the velocity to become single-valued, see Fig. 15. In order to determine the position of the jump from first principles, one solves the viscous Burgers' equation

$$\frac{\partial v}{\partial t} + v v_x = \nu v_{xx}, \tag{85}$$

and takes the limit $\nu \to 0$ [41]. In terms of the potential ϕ, exact solutions of (85) can be found in the form [42]

$$\phi(x,t) = -2\nu \ln \int_{-\infty}^{\infty} \exp\left\{-\frac{G(\eta,x,t)}{2\nu}\right\} d\eta, \tag{86}$$

where

$$G(\eta,x,t) = \phi_0(\eta) + \frac{(x-\eta)^2}{2t}. \tag{87}$$

In the limit $\nu \to 0$, the integral is dominated by the saddle points

$$G_\eta(\xi,x,t) = \phi_0'(\xi) + \frac{x-\xi}{t} = 0.$$

Inserted into (87), this yields

$$G(\xi,t) = \phi_0(\xi) + \frac{\phi_0'(\xi)^2 t}{2}, \quad x = \xi + \phi_0'(\eta)t, \tag{88}$$

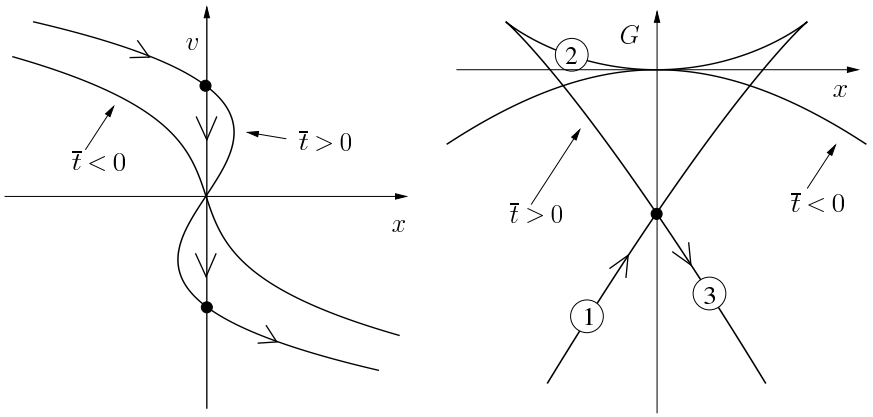

FIG. 15. Shock formation in the inviscid Burgers' equation. On the left, an initially single-valued profile develops into a three-valued s-curve. In a saddle-point approximation, the profile is constructed by moving along the potential, shown on the right. In the multi-valued region, the dominant contribution comes from the most negative value of the potential, leading to a shock position satisfying the equal-area rule.

which is precisely the solution (82) to the potential of the *inviscid* Burgers' equation.

The potential, and thus the saddle point of the integral, is drawn on the right of Fig. 15. For $\bar{t} < 0$ the saddle point is unique, but for $\bar{t} > 0$, inside the cusp region, there are three values to choose from. However clearly, the dominant contribution in the limit $\nu \to 0$ comes from the lowest branch. This means the true solution comes from moving along the branch labeled 1, and then crosses over to the branch 3 at the crossing point. As we have seen, this corresponds to inserting a jump into the s-curve, such that the areas of the two resulting lobes are equal. This is the famous Maxwell's rule for the insertion of a shock [41].

To confirm that (86) indeed reproduces the inviscid solution in the limit $\nu \to 0$, we calculate the velocity:

$$v = \phi_x = \frac{\int_{-\infty}^{\infty} G_x e^{-G/(2\nu)} d\eta}{\int_{-\infty}^{\infty} e^{-G/(2\nu)} d\eta}. \approx G_x(\xi, x, t) \tag{89}$$

In the last step we have used that the saddle point contribution to the integral is

$$\int_{-\infty}^{\infty} g(\eta) e^{-\frac{G(\eta,x,t)}{2\nu}} d\eta \approx g(\xi) \sqrt{\frac{4\pi\nu}{\partial_\xi^2 G(\xi, x, t)}} e^{-\frac{G(\xi,x,t)}{2\nu}},$$

where ξ is a solution of (88). But

$$G_x(\xi, x, t) = \frac{x - \xi}{t} = \phi_0'(\xi)$$

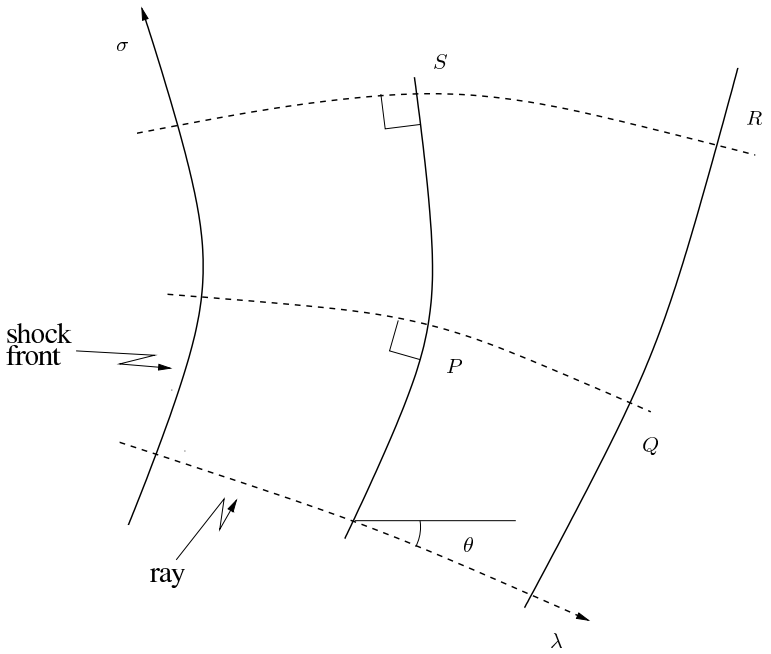

FIG. 16. The "geometrical optics" approximation of shock dynamics. Shock fronts and rays form an orthogonal plane coordinate system (λ, σ); λ measures the distance along rays, σ the distance along a shock front.

at the saddle point, which according to (83) indeed implies that for $\nu \to 0$ (86) is a solution to the inviscid Burgers' equation.

D. Motion of shock fronts

Whitham [42, 43] has developed a simplified theory for the motion of shock fronts, which is based on the ideas of geometrical optics. We introduce an orthogonal curvilinear coordinate system (λ, σ), defined by the advancing shock front (solid lines, constant λ). Another set of curves are called "rays" (dashed lines, constant σ), which are, by definition, orthogonal to the shock fronts. The variable σ labels the position along a shock front; since σ is constant along rays, this defines the value of σ along each front. The position along rays is labeled by the time taken by the shock front to reach a certain position. We normalize time by the vacuum sound speed c_0 ahead of the shock and define $\lambda = c_0 t$.

The problem is written in terms of two dependent variables $M(\lambda, \sigma)$ and $A(\lambda, \sigma)$. The first is the Mach number $M = u_s/c_0$ (u_s is the shock speed), so that $M(\lambda, \sigma)d\lambda$ is the spatial distance along a ray between λ and $\lambda + d\lambda$. The second variable is defined such that

$A(\lambda,\sigma)d\sigma$ is the spatial distance between rays at σ and $\sigma+d\sigma$. Thus $A(\lambda,\sigma)$ measures how the shock front expands and contracts. The physical nature of the problem is determined by an assumed local functional relation $A = f(M)$. Using an analogy with shock-tube dynamics, Whitham [43] considers the form

$$A = f(M) = \chi M^{-\nu}, \tag{90}$$

where χ is a constant and $\nu = 1 + 2/\gamma + \sqrt{2\gamma/(\gamma-1)}$ with γ the adiabatic gas exponent. The choice $f \propto (M-1)^{-2}$ yields geometrical optics [42]. We note that true shock dynamics, as described by the compressible Euler equation, is a non-local phenomenon which cannot be described exactly by a local relation such as (90). However, geometrical shock dynamics is often found to be an excellent approximation when compared to experiment [44] and full numerical simulations [45].

Now from purely geometrical considerations, the equations of motion become

$$\frac{\partial\theta}{\partial\sigma} = \frac{1}{M}\frac{\partial A}{\partial\lambda}, \quad \frac{\partial\theta}{\partial\lambda} = -\frac{1}{A}\frac{\partial M}{\partial\sigma}. \tag{91}$$

As pointed out in [46], this nonlinear set of equations can be solved by performing a hodograph transformation, which exchanges dependent and independent variables. As a result, one obtains a function $\lambda(M,\theta)$, whose equipotential lines represent a solution to the problem at time λ.

To reconstruct the shock front, we can use the formulae

$$x = -\int \kappa^{-1}\sin\theta d\theta, \quad y = \int \kappa^{-1}\cos\theta d\theta, \tag{92}$$

which follow directly from the definition of the curvature $\kappa = d\theta/ds$, to be integrated along $\lambda(M,\theta) = const$. It is straightforward to show [47] that

$$\kappa^{-1} = (\nu+1)\chi^2 M^{-2-2\nu}\left(\frac{\partial\lambda}{\partial M}\right)^{-1} D,$$

where D is the Jacobian of the hodograph transformation. Thus singularities (where $\kappa\to\infty$) are associated with points where the hodograph transformation becomes non-invertible and $D = 0$.

Now let us assume that κ^{-1} vanishes at a point; we can rotate the coordinate system to ensure this is at $\theta = 0$. Then along the shock front, we can write $\kappa^{-1} = a\theta + O(\theta^2)$, which implies

$$x = x_0 - \frac{a\theta^3}{3} + O(\theta^4), \quad y = y_0 + \frac{a\theta^2}{2} + O(\theta^3),$$

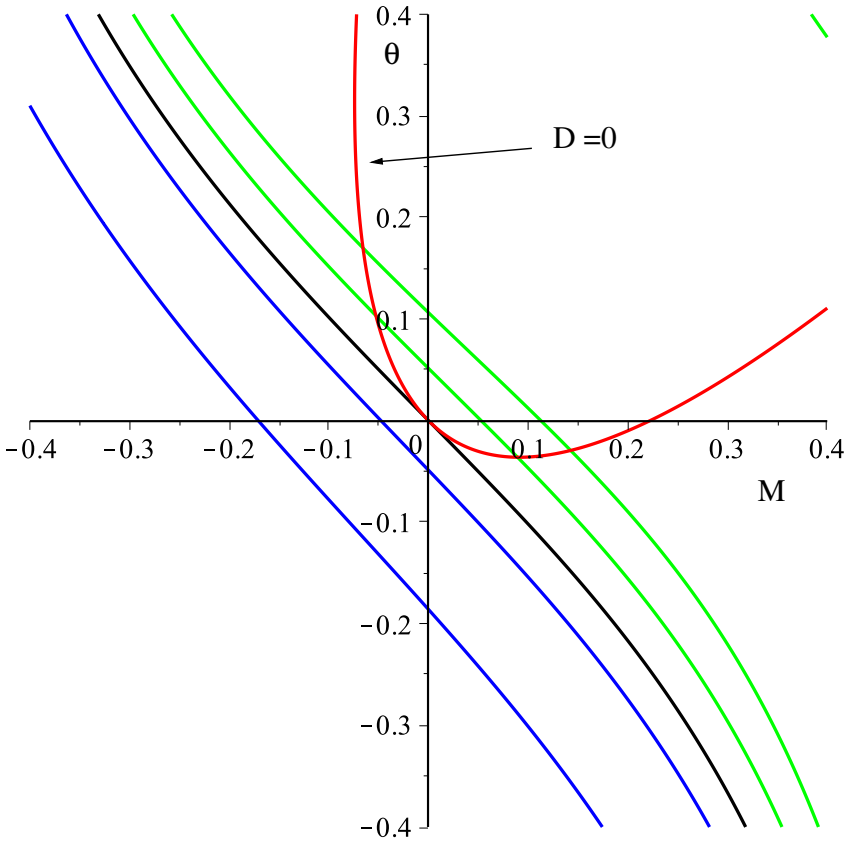

FIG. 17. The formation of a swallowtail. The solution front advances from left to right: blue (before the singularity), black (at the singularity), and green (after the singularity), when the front has two intersections with $D = 0$.

which is a cusp. To understand when this cusp occurs for the first time, we need to consider the structure of the problem in the (M, θ)-plane, see Fig. 17.

The curve $D = 0$ is a line (there may be several distinct lines) in the plane, while the shock front moves in the plane as the time λ varies. If there is no singularity originally, there can be no intersection of the front with the curve $D = 0$. However if an intersection occurs, it is clear geometrically that this must first occur tangentially. But this means that the zero of κ^{-1} must be of higher order, at the time a singularity first occurs. As a result, the curvature (up to a rescaling of time) is of the form

$$\kappa^{-1} = -\lambda + A\theta^2,$$

where the singularity first occurs at $\lambda = 0$ and $A > 0$. Inserting into (92), we obtain the

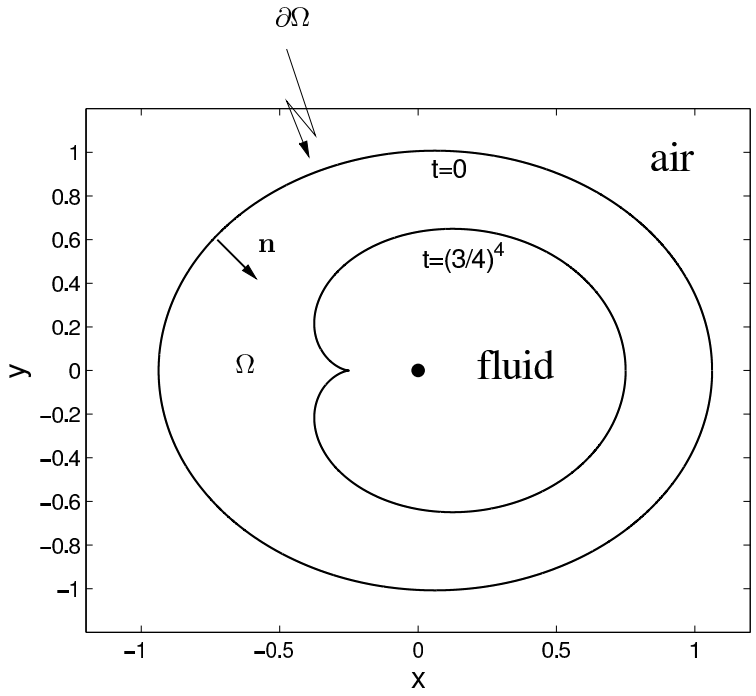

FIG. 18. The formation of a cusp in the Hele-Shaw problem with suction at the origin, using the exact solution (97) with coefficients (98). The initial condition is $a_1(0) = 1$, $a_2(0) = 1/16$. A cusp is formed at $t = (3/4)^4$.

swallowtail

$$x = \lambda\theta^2/2 - A\theta^4/4, \quad y = -\lambda\theta + A\theta^3/3. \tag{93}$$

which was shown already in Fig. 9. The left curve shows the shock front before the singularity ($\lambda < 0$), on the right two cusps have formed ($\lambda > 0$). The position of the cusps correspond to intersections of the front with the curve $D = 0$ in the hodograph plane, as shown in Fig. 17.

E. Hele-Shaw flow without surface tension

A Hele-Shaw cell consists of two closely spaced glass plates, partially filled with a viscous fluid. The problem is to find the time evolution of the free interface between fluid and gas. Here we consider the case that the fluid occupies a closed two-dimensional domain Ω. Within Ω, the pressure obeys $\Delta p = 0$, with boundary conditions

$$p = 0, \quad v_n = -\nabla p \cdot \mathbf{n} \tag{94}$$

on the free surface $\partial\Omega$, where v_n is the normal velocity. The geometry is illustrated in Fig. 18: an initially smooth patch of viscous fluid is surrounded by air, occupying a region Ω, with boundary $\partial\Omega$. The flow is driven by a point sink of strength m placed inside the fluid. As the fluid is sucked out and the fluid patch shrinks, its boundary forms a cusp singularity in finite time, whose structure we aim to investigate.

As described in detail in [5], the problem can be solved [48–51] introducing the conformal mapping

$$z = f(\xi, t), \quad \xi = re^{i\theta}, \tag{95}$$

which maps the circle $|\xi| = 1$ onto $\partial\Omega$, resulting in the equation of motion

$$\mathrm{Re}\,(\overline{\mathrm{z_t}}\xi \mathrm{z}_\xi) = -\frac{\mathrm{m}}{2\pi}. \tag{96}$$

Solutions to (96) can be found in the form of a polynomial

$$f(\xi) = \sum_{i=1}^{n} a_i(t)\xi^i, \tag{97}$$

where the coefficients have to satisfy a set of ODE's found by inserting into (96). For example, in the simplest case $n = 2$ the equations are

$$a_1\dot{a}_1 + 2a_2\dot{a}_2 = -\frac{m}{2\pi}, \quad a_1\dot{a}_2 + 2a_2\dot{a}_1 = 0, \tag{98}$$

which can easily be integrated for general initial conditions [5]. The particular case of initial conditions $a_1(0) = 1, a_2(0) = 1/16$ is shown in Fig. 18, which leads to the formation of a generic 3/2 cusp (36).

The formation of the cusp is associated with the mapping $z = f(\xi)$ no longer being invertible on $|\xi| = 1$, so that a self-intersection occurs. The simplest such case occurs when $f' = 0$ on the unit circle; then up to a complex rotation, we can assume that

$$f = (\xi - \xi_0)^2, \quad \xi_0 = 1 + \epsilon. \tag{99}$$

This means that the point of non-invertability lies outside of the unit circle for $\epsilon > 0$, and approaches the unit circle as $\epsilon \to 0$. Indeed, inserting (99) into (95) yields

$$x = \epsilon^2 + (-1 + \epsilon)\theta^2 + O(\theta^4), \quad y = -2\epsilon\theta + (-1 + \epsilon/3)\theta^3 + +O(\theta^5), \tag{100}$$

which is a cusp that unfolds for $\epsilon \neq 0$.

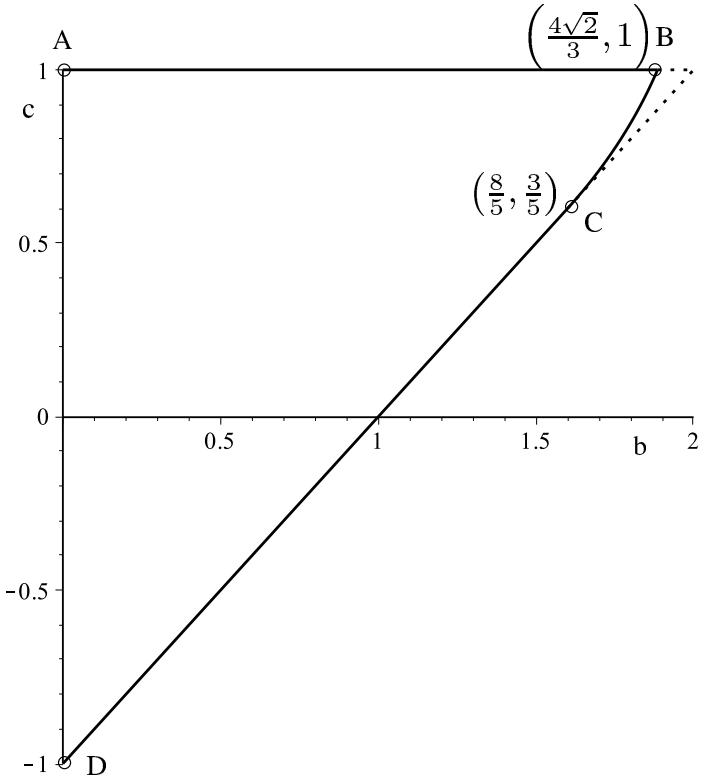

FIG. 19. The region over which the mapping (101) remains univalent for $b > 0$. Between B and C, the curve is $b^2/4 + 4\,(c/3 - 1/2)^2 = 1$. Between A and B, there are two cusps $f' = 0$ at $\xi = -b/2 \pm i\sqrt{4 - b^2}/2$, between C and D there is a single cusp $f'(-1) = 0$. Between B and C, two sides of the interface touch to enclose a bubble.

Higher order zeroes lead to higher order singularities, for example $f = (\xi - 1)^n$ leads to the germ θ^n, θ^{n+1}. Other germs, such as θ^2, θ^5, can be realized as well, and describe the formation of a small bubble, as seen in Fig. 7. This can be illustrated using the solution (97) for $n = 3$, which can be written

$$f(\xi) = a\left(\xi + b\xi^2/2 + c\xi^3/3\right). \tag{101}$$

Physically permissible solutions must be complex differentiable and invertible or *univalent* on the unit disk $\xi \leq 1$ [52]. In the plane (b, c), the region of univalency is shown in Fig. 19 for $b > 0$; the figure is mirror-symmetric with respect to the $b = 0$ axis.

Along the boundaries formed by straight lines, f' vanishes on the unit circle, where the boundary of the fluid domain develops one or two cusp singularities. Along the ellipsoidal boundary between B and C, the boundary touches so as to enclose a bubble. As C is

approached, the size of the bubble goes to zero, so asymptotically the shape must be a similarity solution of the form (39). Accordingly at C, the boundary forms a 2/5 cusp singularity. On the other hand at B, the interface encloses a bubble with two cusps as shown in Fig. 10, except that the asymptotic form (46) is valid only in the limit of vanishing bubble size. To realize this, another parameter would be necessary, for example the solution with (97).

As one moves away from the boundary of the univalency domain, the singularities described above unfold. An analysis of the flow lines of the equations of motion shows that solutions end on the boundary, so all the singularities described above are realized by the dynamics.

F. Two-dimensional Stokes flow

Here the flow is governed by the Stokes equation, which in two dimensions can be written in terms of the stream function ψ, with $u = \psi_y$ and $v = -\psi_x$. The stream function obeys the biharmonic equation $\triangle^2\psi = 0$. In a stationary state, which we are considering, the surface of the fluid is a line with $\psi = const.$ On this surface, we also have the surface stress condition

$$\sigma_{ij}n_j = \gamma\kappa n_i, \tag{102}$$

where γ is surface tension and κ the curvature of the interface. Once more the flow can be driven by singularities, such as sources and sinks, or a vortex dipole [21].

A complex formulation of this problem was developed by Richardson [53]. The stream function is written as

$$\psi = Im(\phi(z) + \overline{z}\chi(z)), \tag{103}$$

where ϕ and χ are analytic functions. The boundary conditions at the free surface can be shown to be

$$Im\left[\left(\overline{\frac{dz}{ds}}\right)\phi(z) + \overline{z}\chi(z)\right] = \frac{\gamma}{4\eta}, \quad \phi(z) + \overline{z}\chi(z) = 0, \tag{104}$$

where η is the viscosity of the fluid. The idea is to find time-dependent solutions using the map (95). The functions ϕ, χ have to satisfy boundary conditions at the position of any singularities in the flow domain. The general, time-dependent case is too complicated to be solved in general, but progress can be made in particular cases, as described below.

1. Time-dependent flow without surface tension

In the absence of surface tension ($\gamma = 0$) solutions can be found in the polynomial form (97), see [52, 54]. The idea is to write down equations of motion for the moments

$$C_k(t) = \int_{\Omega(t)} \zeta^k(z,t) dx dy = \frac{1}{2i} \int_{|\zeta|=1} \zeta^k f'(\zeta,t) \overline{f}(1/\zeta,t) d\zeta$$

using (104), which results in a system of ODE's. The moments can then be calculated in terms of the polynomial coefficients a_i, all C_k with $k > n-1$ being zero. Then the same reasoning can be applied to polynomial solutions as done previously for the case of Hele-Shaw flow.

2. Stationary flow with surface tension

Another interesting class of solutions obtained using the formulation (104) and complex mapping involves two-dimensional Stokes flow with surface tension being driven by prescribed singularities in the flow to reach a steady state, which reflects a balance between the viscous driving and surface tension. The first such solution was found in [21], where a vortex dipole of strength α is located at a distance d below a free surface of infinite extend. This solution was generalized to include other singularities below an infinitely extended free surface [55–57], and the stationary state of a two-dimensional bubble in a driven viscous flow [58, 59], as well as two interacting bubbles [59]. All of these solutions lead to generic 2/3 cusps, rounded by surface tension. Using additional control parameters, one can presumably generate higher order singularities.

In [21], the amount of deformation of the free surface by the viscous flow is measured by the capillary number

$$Ca = \frac{\alpha \eta}{d^2 \gamma}, \tag{105}$$

which measures the ratio of viscous forces over surface tension forces. The solution of the problem is too involved to be presented here in full. However, the exact surface shape, in units of d, is given by the simple mapping

$$x = a\cos\theta + (a+1)\frac{\cos\theta}{1+\sin\theta}, \tag{106}$$

$$y = a(1+\sin\theta). \tag{107}$$

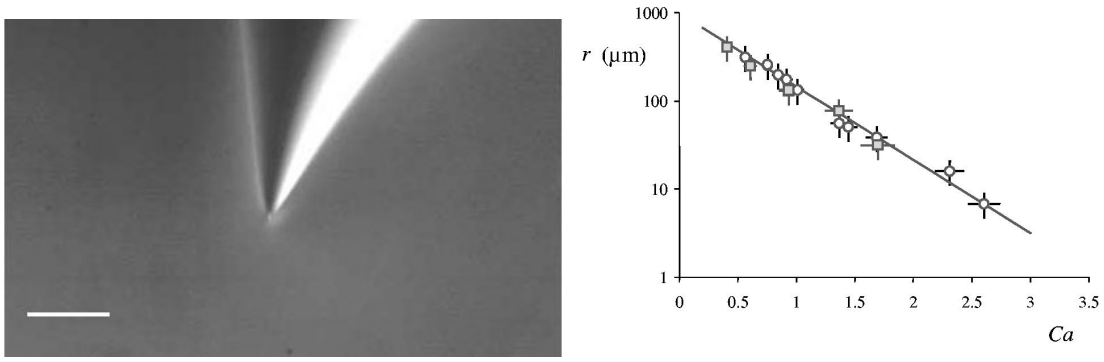

FIG. 20. Experimental data on the cusping of a viscous fluid, taken from [60]. On the left, a closeup of the tip of a cusp on the surface of a viscous fluid; the scale bar corresponds to 200 μm. On the right, the radius of curvature of the (almost) cusp as function of capillary number. In agreement with (113), the dependence is exponential.

The parameter a is determined from the equation

$$4\pi Ca = \frac{-a(3a+2)^2 K(m)}{1+a+\sqrt{-2a(a+1)}}, \tag{108}$$

where

$$m = \frac{2}{(-2a/(a+1))^{1/4} + ((a+1)/(-2a))^{1/4}} \tag{109}$$

and K is the complete elliptic integral of the first kind:

$$K(m) = \int_0^{\pi/2} \frac{d\theta}{\sqrt{1-m^2\sin^2\theta}}. \tag{110}$$

In (108) we have only reported the form of the equation for the more relevant case $Ca > 0$. Asymptotic analysis of (108)-(110) reveals that for large Ca,

$$a = -\frac{1}{3} + \epsilon, \quad \epsilon \approx \frac{32}{9}\exp\left\{-16\pi Ca\right\}. \tag{111}$$

It is easy to confirm that (106) yields a cusp for $a = -1/3$, i.e. for $Ca = \infty$ or vanishing surface tension. If one expands around the cusp point by putting $\theta = \pi/2 + \delta$, one obtains

$$x = -\frac{2\epsilon}{3}\delta - \frac{\delta^3}{12}, \quad y + \frac{2}{3} - 2\epsilon = \frac{\delta^2}{6}, \tag{112}$$

which is the generic unfolding (36) of the cusp. As is apparent from Fig. 6, the case $\epsilon < 0$ leads to self-intersection of the free surface, which is of course not physical. The radius of curvature of the cusp for $\epsilon > 0$ is given by

$$R \approx \frac{256}{3}\exp\left\{-32\pi Ca\right\}, \tag{113}$$

as found from (112),(111). The exponential dependence (113) has been confirmed experimentally (cf. Fig. 20).

G. Time-dependent flows with surface tension

Another class of exact two-dimensional Stokes flow solutions are those driven primarily by surface tension, leading to a time dependent flow [61–68]. In general, in the absence of driving, the dynamics will lead to a smoothing of singularities [67, 68], and will only lead to near cusps for very particular initial conditions [66]. On the other hand, cusp singularities can be imposed through the initial condition, for example the cusp which is produced when two surfaces touch [61–65]. However, this cusp will generically be of 1/2 power law type, which cannot be described by a smooth function. In other words, while (t^2, t^3) describes a cusp, (t, t^2) is a smooth function, not a cusp. As we will see in two different examples below, a 1/2 cusp can only be realized as the singular limit of smooth mappings, and singularity theory does not allow to classify it.

1. A counterexample: merging of two cylinders

A general solution to the Stokes flow problem with surface tension can be written in the form

$$f(\xi, t) = \xi \left(\frac{Ba}{1 - a\xi} + \frac{Cb}{1 + b\xi} \right), \tag{114}$$

where a, b, B and C are functions of t. The speed of coalescence is set by the capillary-viscous velocity $v_\eta = \gamma/\eta$. If $a = b$ and $B = C > 0$, then the domain presented by (114) is also symmetric about the y-axis and the initial conditions $a = b = 1$ at $t = 0$ describe two touching circular discs. In that case, (114) can be written as

$$f(\xi, t) = \sqrt{\frac{A}{\pi}} \frac{1 - a^4}{\sqrt{1 + a^4}} \frac{\xi}{1 - a^2\xi^2}, \tag{115}$$

where A is the total area of the domain and a varies with time as follows:

$$t = \frac{\sqrt{A\pi}}{2v_\eta} \int_{a^2}^{1} \frac{dp}{p\sqrt{1 + p^2}K(p)}. \tag{116}$$

Clearly, at the initial time $t = 0$, the parameter is $a = 1$, and $a \to 0$ for $t \to \infty$. For $a = 0$, the map becomes $z = \sqrt{A/\pi}\xi$, which is a circle of radius $\sqrt{A/\pi}\xi$.

The limit $a \to 1$, on the other hand, is non-uniform, and $z \to 0$ for any $\xi \neq \pm 1$. Expanding about $\xi = 1$ corresponds to expanding about $\theta = 0$; taking the first few leading terms in θ and $\delta = 1 - a$ we find

$$\frac{z}{R} = 2\left(1 + i\frac{\theta}{\delta} + \dots\right),$$

where $R = \sqrt{A/(2\pi)}$ is the radius of one of the initial cylinders. This indicates that $\theta \propto \delta$ in the limit $\delta \to 0$, so we define $\theta = \phi\delta$. Taking the leading terms in this limit, the result is

$$\frac{z}{R} = 2\left(\frac{1}{1+\varphi^2} + i\frac{\varphi}{1+\varphi^2}\right) + O(\delta). \tag{117}$$

This is a circle of radius 1 centered at $x/R = 1$, corresponding to one of the initial cylinders; the other is found by expanding about $\xi = -1$. The tip of the cusp is reached in the limit $\varphi \to \infty$, where the map is singular.

It is also instructive to consider the neighborhood of the point $x = 0$, where the two cylinders join, and where for $\delta > 0$ there is a local minimum of $y(x)$. Putting $\xi = ie^{i\varphi}$ this corresponds to $\varphi = 0$, and in units of the minimum radius of the neck $R_m \approx \sqrt{A/\pi}\delta$ one finds

$$\frac{x}{R_m} = -\delta\frac{\sin\varphi}{\cos^2\varphi} + O(\delta^2), \quad \frac{y}{R_m} = \frac{1-\cos\varphi}{\cos\varphi} + O(\delta^2),$$

which is a parabola. Note that the x-component vanishes as $\delta \to 0$, reflecting the singular nature of this limit.

H. Stationary two-dimensional potential flow without surface tension

Inviscid potential fluid flow is governed by the equations

$$\mathbf{u} = \nabla\phi, \quad \triangle\phi = 0, \tag{118}$$

where ϕ is the velocity potential. The free surface is convected by the fluid velocity, and the free surface is at constant pressure. We consider the simplest case of steady flow, as well as of no body or surface tension forces. According to Bernoulli's equation, the fluid speed then has to be constant on the free surface.

Exact solutions to the flow problem can be found if the fluid domain is bounded by free surfaces and straight solid boundaries alone [69], by mapping the fluid domain onto the upper half of the complex plane, which we denote by ζ. To find a greater variety of solutions,

the flow can be driven by placing singularities (like vortices, sources, and sinks) inside the flow. To this end, one introduces the complex potential $w = \phi + i\psi$, where ψ is the stream function. Following [70], the derivative of the mapping function is written in the form

$$\frac{dz}{d\zeta} = \frac{dz}{dw}\frac{dw}{d\zeta} = e^{\Omega}\frac{dw}{d\zeta}. \tag{119}$$

Hopkinson [71] observed that the complex velocity $dw/d\zeta$ has to be real on the real ζ-axis, while Ω has to be purely imaginary on a free surface; both conditions can be satisfied using the method of images. Singularities on the free surface arise when there is a stagnation point on the free surface, i.e. a zero of $dw/d\zeta$. Taking this zero to be at $\zeta = 0$, we have

$$\frac{dw}{d\zeta} = A\zeta\left(1 + a\zeta\right), \quad \Omega = i(\Omega_0 + \Omega_1\zeta) + O(\zeta^2); \tag{120}$$

owing to the boundary conditions on the real axis (which corresponds to the free surface), all parameters A, a, Ω_0, Ω_1 must be real. Then expanding to leading order and integrating, one obtains

$$z = Ae^{i\Omega_0}\left[\frac{\zeta^2}{2} + (a + i\Omega_1)\frac{\zeta^3}{3}\right],$$

and it is easy to see that $(x(\zeta), y(\zeta))$ for ζ real is a cusp.

Note that the cusp does not arrive through a gradual sharpening of the tip (it does not unfold as in (112) or (100)). This is because the boundary condition forbids zeros $dw/d\zeta = \zeta - i\epsilon$ near the real axis, since $dw/d\zeta$ would not be real. As a result, one cannot have a zero approach the real axis, which would correspond to an unfolding. Instead, the only way a cusp can be created is through a higher-order zero separating into two zeroes, which corresponds to the unfolding of a swallowtail, as shown in Fig. 9; as a result, two cusps are created. This bifurcation corresponds to

$$\frac{dw}{d\zeta} = \zeta^2 - \epsilon^2 = (\zeta - \epsilon)(\zeta + \epsilon), \quad \Omega = i(\Omega_0 + \Omega_1\zeta) + O(\zeta^2),$$

with ϵ being the unfolding parameter.

There is a very special potential flow solution in the presence of gravity [72–74], in which liquid is layered above a two-dimensional ridge. A local analysis shows that a 2/3 cusp is formed [20]; this is not surprising, since gravity is not expected to change the local behavior near a cusp.

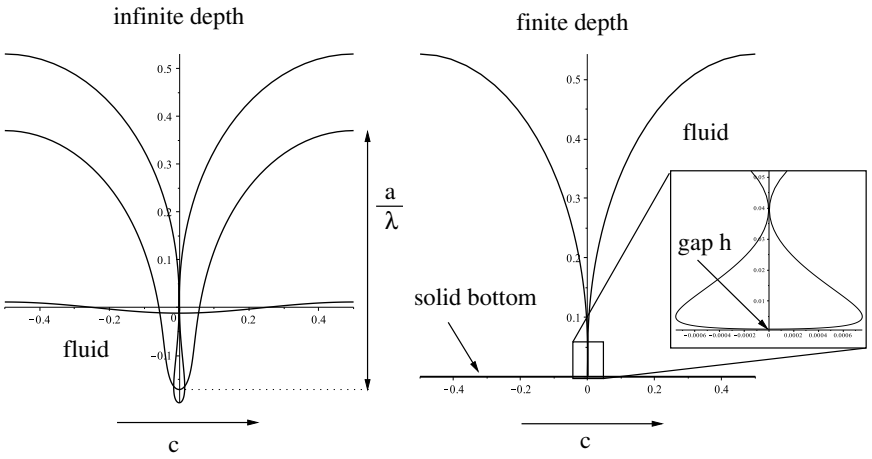

FIG. 21. Waves traveling at speed c on a quiescent fluid, as described by (121). On the left, the fluid is of infinite depth for $B = 4, 1$, and $B = B_c = 0.78818\ldots$, while on the right, the x-axis is a solid bottom. For infinite depth, the profile self-intersects at a critical amplitude. For finite depth, we show the profile (122), (123) for $k = 0.9$ and $B = 0.8731$, for which a bubble is formed. In the limit $k \to 1$ the size of this bubble goes to zero.

I. Counterexample: Traveling wave over solid bottom

In the previous section we described driven cusps in potential flow without surface tension. One might think that the introduction of surface tension will lead to a rounding, as it does in the viscous case (112). Using complex mapping techniques, Crapper [75] found the shape of a nonlinear wave at finite surface tension γ, traveling at speed c on a fluid of infinite depth in potential flow. Thus $L = \gamma/(\rho c^2)$ is a characteristic length scale of the problem. The shape of the free surface, in units of wavelength $\lambda = 2\pi L \tanh B$, is

$$x = \frac{1}{2\pi}\left[\phi - \frac{2\sin\phi}{\cosh B + \cos\phi}\right], \quad y = \frac{1}{2\pi}\left[\frac{2\sinh B}{\cosh B + \cos\phi} - 2\right], \tag{121}$$

where B is a parameter; the minimum is at $\phi = 0$. The relative amplitude is $a/\lambda = 2/(\pi \sinh B)$, which goes to zero for $b \to \infty$. However, for $B > B_c = 0.78818\ldots$ there will be a self-intersection, as seen on the left of Fig. 21.

Physically, the reason is that a cusp would imply an upward force of 2γ, which must be counterbalanced by a localized minimum of the Bernoulli pressure. But although the speed of the flow past the free surface is maximum at the trough, so according to Bernoulli is a minimum of the pressure, this is not sufficiently localized to produce a point cusp. On the

other hand, if the same calculation is repeated with a solid bottom, and the gap h between the trough and the bottom becomes small, the velocity becomes large in a small region. As shown on the right of Fig. 21, one can produce smaller and smaller bubbles as the gap h goes to zero. Writing all lengths in units of the wavelength $\lambda = 4L\mathrm{sn}(B,k')\mathrm{cd}(B,k')\kappa$ from now on, the generalized exact solution over a solid bottom [76] becomes

$$x = \frac{1}{4\kappa}\left[2E(\mathrm{am}(\phi,k),k) - k'^2\phi - 2k^2\mathrm{sn}(\phi,k)\mathrm{cd}(\phi,k) + \frac{2kk'^2\mathrm{sd}(\phi,k)\mathrm{nd}(\phi,k)}{\mathrm{dn}(B,k') - k\mathrm{cd}(\phi,k)}\right] - \frac{1}{2}, \tag{122}$$

$$y = \frac{1}{4\kappa}\left[(1+k^2)B - 2E(\mathrm{am}(B,k'),k') + \frac{2k'^2\mathrm{sn}(B,k')\mathrm{cn}(B,k')}{\mathrm{dn}(B,k') - k\mathrm{cd}(\phi,k)}\right], \tag{123}$$

where $\kappa = 2E(k) - k'^2K(k)$ and $k' = \sqrt{1-k^2}$; we are using the notation of [77] for the elliptic integrals, Jacobi elliptic functions, and Jacobi amplitude. A full period of the wave is covered by the range $0 \le \phi \le 4K(k)$, where the trough lies at $\phi = 2K(k)$. In the range $K \le \phi \le 3K(k)$, the elliptic integral is to be continued as $E(\mathrm{am}(\phi,k),k) = 2E(k) + E(\mathrm{am}(\phi - 2K(k),k),k)$, and the rest can be recovered by using the period of $4K(k)$ of the Jacobi elliptic functions.

The solution (122),(123) has the two parameters k and B, which permit to prescribe the amplitude a of the wave and the spacing h between the minimum and the bottom according to

$$a = \frac{1}{2}\mathrm{sc}(B,k') \tag{124}$$

and

$$h = \frac{1}{4\kappa}\left[(1+k^2)B - 2E(B,k') + 2\mathrm{sc}(B,k')(\mathrm{dn}(B,k') - k)\right]. \tag{125}$$

We investigate the limit of small gap $h/\lambda \to 0$ while a/λ remains finite, i.e. $k \to 1$. We expect the profile near the solid bottom to assume a singular shape.

Taking the limit $k' \to 0$ leads to an equation for an ellipse ($\kappa \approx 2$):

$$x = \frac{1}{2}\frac{\sinh\phi\cosh\phi}{\cosh^2\phi - \sin^2 B} - \frac{1}{2}, \quad y = \frac{1}{2}\frac{\sin B\cos B}{\cosh^2\phi - \sin^2 B}. \tag{126}$$

Here $\phi = 0$ corresponds to the crest of the wave at $x = -1$, while in the limit $\phi \to \infty$ the minimum is reached for $x = y = 0$, i.e. the wave touches the wall; the right of the minimum can be recovered by symmetry. For small x the profile is linear:

$$y = \pm\tan 2Bx, \tag{127}$$

which means that at $x = 0$ there is a *corner*, a reflection of the singular limit we are taking.

We are interested in taking the limit in such a way that a bubble is inclosed, as shown in the inset on the right of Fig. 21. By construction, this means that a cusp is formed, and the profile becomes vertical, corresponding to the limit $B \to \pi/4$ in (127). If the wave profile were to remain smooth in the limit, it would follow from the arguments of Section IV A that the cusp has a 2/5 power, and is described by the scaling function (39). However, for $B = \pi/4$, (126) becomes the equation of a circle, so near the cusp tip the profile is

$$x = y^2, \tag{128}$$

a 1/2 cusp, which does not appear within the singularity theory framework. We now aim to describe the bubble at the end of the tip, in the limit $k \to 1$; the condition that the two sides of the profile touch amounts effectively to a condition on $B = B(k)$. To that end, we have to describe the profile near the minimum at $\phi = 2K(k) \to \infty$ for $k \to 0$. To find a regular expansion, we shift the origin to zero: $\phi \to \phi + 2K$, to obtain

$$x = \frac{1}{4\kappa}\left[2E(\phi,k) - k'^2\phi - 2k^2\mathrm{sn}(\phi,k)\mathrm{cd}(\phi,k) - \frac{2kk'^2\mathrm{sd}(\phi,k)\mathrm{nd}(\phi,k)}{\mathrm{dn}(B,k') + k\mathrm{cd}(\phi,k)}\right], \tag{129}$$

$$y = \frac{1}{4\kappa}\left[(1+k^2)B - 2E(B,k') + \frac{2k'^2\mathrm{sn}(B,k')\mathrm{cn}(B,k')}{\mathrm{dn}(B,k') + k\mathrm{cd}(\phi,k)}\right]. \tag{130}$$

To find the inner asymptotics, we expand (129),(130) in a power series in $\epsilon = k'^2/8$,

$$x = \frac{1}{\kappa}\sum_{i=2}^{\infty} x_i\epsilon^i, \quad y = \frac{1}{\kappa}\sum_{i=2}^{\infty} y_i\epsilon^i, \tag{131}$$

using series expansions of the Jacobi elliptic functions in k' inspired by [78]; this yields to leading non-vanishing order

$$x = \frac{\epsilon^2}{\kappa}\left[2\phi + \cos 2B \sinh 2\phi\right], \quad y = \frac{\epsilon^2}{\kappa}\left[2B + \sin 2B \cosh 2\phi\right]. \tag{132}$$

This has a quadratic minimum with curvature proportional to $1/k'^4$, while for large ϕ one recovers the linear behavior (127), which matches the outer solution.

However, for $B = \pi/4$ the linear behavior (127) becomes singular, which means we have to expand to higher order in ϵ, and to consider corrections $B = \pi/4 + \delta$, where δ is a small parameter. Considering the leading order expressions in δ only, we find

$$x_3(\phi,\pi/4) = 8\phi + \pi\sinh(2\phi) + O(\delta), \tag{133}$$

$$x_4(\phi,\pi/4) = \frac{1}{4}\left[-16\pi\phi\cosh(2\phi) + 34\pi\sinh(2\phi) + 164\phi + \sinh(4\phi)\right] + O(\delta), \tag{134}$$

so that for large ϕ the contributions to x behave like

$$x \approx \frac{\epsilon^4 e^{4\phi}}{16} \approx y^2,$$

which matches the outer solution (128). To achieve this, we had to go to fourth order in the expansion in ϵ.

Using this insight, we now consider the limit $\epsilon \to 0$ in such a way that a bubble is enclosed. We will see below that on the scale of the bubble, $e^{-2\phi} \sim \epsilon$, so it is sufficient to consider (133),(134) in the limit $\phi \to \infty$, which means that $x_3 \approx \pi e^{2\phi}/2$ and $x_4 \approx e^{4\phi}/8$. On the other hand, we take into account terms of order δ in the expression for x_2, since the dominant term cancels for $B = \pi/4$. Thus $x_2 \approx 2\phi - \delta e^{2\phi}$, so we expect $\delta \sim e^{-2\phi} \sim \epsilon$. In other words, in the limit of $\epsilon \to 0$ the solution on the scale of the bubble is

$$x = \left(\phi - \frac{\delta}{2} e^{2\phi}\right)\epsilon^2 + \frac{\pi e^{2\phi}}{4}\epsilon^3 + \frac{e^{4\phi}}{16}\epsilon^4, \quad y = \left(\frac{\pi}{4} + \frac{\cosh(2\phi)}{2}\right)\epsilon^2, \tag{135}$$

where now all contributions are consistently of order ϵ^2.

Using (135) and putting $\delta = a\epsilon$, the conditions $x = 0$, $\partial x/\partial\phi = 0$ for the two sides of the profile to touch lead to

$$\frac{1}{2} - \phi_c + \frac{e^{4\phi_c}\epsilon^2}{16} = 0 \tag{136}$$

for the critical value of $\phi = \phi_c$ at which pinch-off occurs. This equation can be solved perturbatively as

$$\phi_c = \frac{\tilde{\epsilon}}{4} + \frac{\ln\tilde{\epsilon}}{4} + \frac{\ln\tilde{\epsilon} - 2}{4\tilde{\epsilon}} + O\left(\frac{1}{\tilde{\epsilon}^2}\right), \quad \delta = \epsilon\left[\frac{\tilde{\epsilon}^{1/2}}{2} + \frac{\pi}{2} + \frac{\ln\tilde{\epsilon}}{4\tilde{\epsilon}^{1/2}} + O\left(\tilde{\epsilon}^{-3/2}\right)\right], \tag{137}$$

with $\tilde{\epsilon} = -2\ln(\epsilon/2)$. This result is compared to numerics in Fig. 22, with very good agreement.

The size of the bubble is determined by the height at the pinch point y_c, and the position x_b, y_b of the maximum at the base, which to leading order become

$$y_c \approx \frac{\epsilon}{2}\sqrt{\tilde{\epsilon}}, \quad x_b \approx \frac{\tilde{\epsilon}\epsilon^2}{4}, \quad y_b \approx \frac{\epsilon}{2\sqrt{\tilde{\epsilon}}}. \tag{138}$$

Clearly $y_b \ll y_c$ in the limit, so the bubble becomes very flat at its base. Introducing similarity variables $X = \tilde{x}/x_b$ and $Y = \tilde{y}/y_c$ (so that the lower half of of the bubble becomes squashed to zero), the shape of the bubble becomes

$$X = 1 - 2Y + Y^2, \tag{139}$$

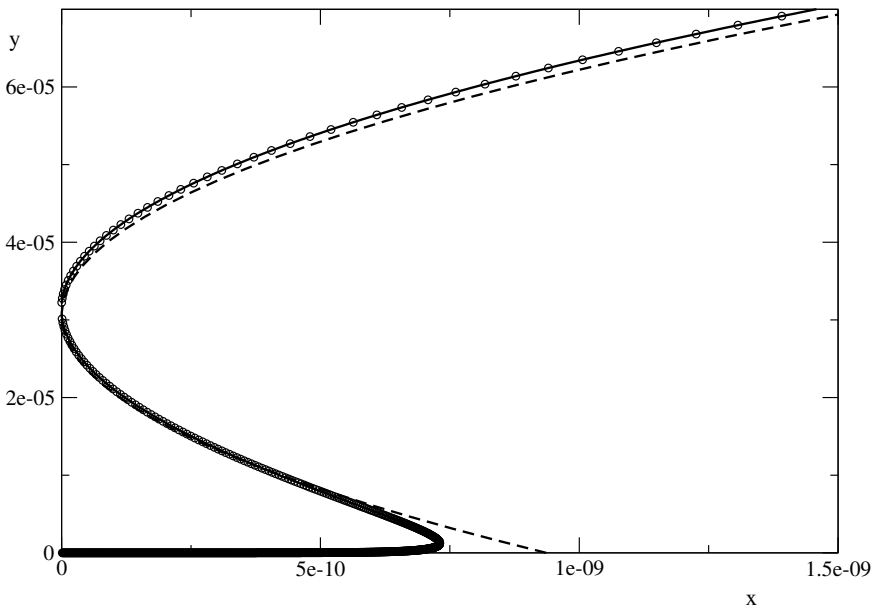

FIG. 22. The neighborhood of the bubble for $k' = 10^{-2}$. The solid line is the full solution (129),(130), with B adjusted such that pinch-off occurs (both sides of the profile touching). The symbols are the asymptotic result (135), with δ determined by (137). The dashed line is the scaling function (139)

which is shown as the dashed line in Fig. 22. Note the appearance of scaling factors $\sqrt{-2\ln\epsilon/2}$, which is reminiscent of the very slow approach to the asymptotic limit seen in inviscid bubble pinch-off [79].

VI. CONCLUSIONS

When thinking about singularities of PDE's, most often one considers them from the point of view of functions becoming non-smooth, i.e. no longer possessing derivatives of arbitrary order. It is therefore remarkable that many singularities, as we have seen, can be described within the framework of smooth mappings. In a sense described before, these singularities are geometrical in nature. Another type of such geometrical singularities, not considered here, are vortices [5, 80]

The most obvious extension of the present review is to curves in space, and in particular to surfaces (two-dimensional objects in three-dimensional space). Within catastrophe theory, this generalization does not present much of a problem, and has been worked out fully in

optics [39, 81]. For the description of shocks in higher dimensions a potential is not available, so that catastrophe theory is not applicable directly. However, our understanding of the structure of the singularity taking from these theories can form the basis for a description based on the equations of motion [82–84].

Moving beyond wave problems to free surface equations is much more challenging, since most solutions in terms of mappings come from the complex domain, and thus are usually confined to two dimensions. However, even in the absence such solutions, an important aspect is that singularity theory provides us with inspiration for the possible structure of solutions. For example, one might guess how the viscous free-surface singularity (112) is "unfolded" into the third dimension in a manner similar to shocks in two and three dimensions [83]. What is needed are rigorous asymptotic arguments, based on the equations, which allow for such an extension.

Appendix A: Invariants of plane curve germs

As we have seen in Section III, any possible germ of a plane curve can be represented in the form (16). However, under an equivalency transformation the sequence of exponents appearing in (16) will in general change. On the other hand, certain properties of a germ will not change, and are called *invariants*. Clearly, they aid in classifying different types of singularities, although in general they are not enough for a complete classification.

As a first step, we define the so-called Puiseux exponents (invariants), which are chosen in such a way that no common factor exists between different exponents, and which could easily be eliminated by substitution. This is ensured by the following algorithm: define β_1 to be the smallest exponent appearing in $y(t)$, which is not divisible by m. If no such exponents existed, it would mean that y is a power series in x and the curve is regular. Now define $e_1 = hcf(m, \beta_1)$ (the highest common factor), and β_2 as the smallest exponent appearing in $y(t)$ and not divisible by e_1. Defining $e_2 = hcf(e_1, \beta_2)$, it is clear that $e_2 < e_1$. Proceeding inductively, we obtain the strictly decreasing sequence of integers $m > e_1 > e_2 > \cdots > e_i > \cdots$, which means there is an integer g such that $e_{g-1} \neq 1$ and $e_g = 1$, called the genus of

the curve. More formally, we have defined

$$\begin{aligned} e_0 &= \beta_0 = m, \\ \beta_{i+1} &= \min\{k \mid c_i \neq 0,\ e_i \nmid k\} \\ e_i &= hcf(e_{i-1}, \beta_i) \end{aligned} \tag{A1}$$

which satisfies $\beta_1 = n$. The integers $\beta_0, \beta_1, ..., \beta_g$ are called the Puiseux characteristic exponents or the Puiseux characteristics of the curve f, and are denoted by $\mathrm{ch}(f)$, and the parameterization of f can be rewritten as:

$$x = t^{\beta_0}, \quad y = \sum_{i=\beta_1}^{\beta_2 - 1} c_i t^i + \cdots + \sum_{i=\beta_{g-1}}^{\beta_g - 1} c_i t^i + \sum_{i \geq \beta_g} c_i t^i, \tag{A2}$$

where the coefficients $c_{\beta_1}, \cdots c_{\beta_g} \neq 0$. From the definition of characteristic exponents we can deduce that the coefficients in above parameterization have the following property: if i and k are integers such that $\beta_{j-1} < k < \beta_j$ and if e_{j-1} does not divide k then the coefficient $c_k \neq 0$. A parameterization of the form (A2) is called a "good" parameterization. The set of Puiseux exponents forms an invariant of the curve since if one were to perform any diffeomorphic transformation on (A2), after repeating the above procedure one arrives at the same set of exponents.

Another invariant sequence of numbers, characterizing topological and analytical properties of a curve, is the semigroup, introduced in Section III for special cases. We will motivate its construction in a heuristic fashion below, as the set of intersection numbers of a curve f with other curves in the plane, in the following sense: Suppose a curve f_1 is given by the equation $g(x, y) = 0$, and a curve f_2 by a good parameterization $(x, y) = (\phi(t), \psi(t))$, such that $\phi(0) = \psi(0) = 0$. Then the intersection number of f_1 and f_2 at the origin is defined as the order of the zero of g, written as function of t, at the origin:

$$i(f_1, f_2) = \mathrm{ord}(g(\phi(t), \psi(t))). \tag{A3}$$

The reason is that if one perturbs the leading-order term $t^{i(f_1,f_2)}$, the maximum number of zeroes is the intersection number. Hence $t^{i(f_1,f_2)}$ measures the maximum number of local intersections between the curves as they are perturbed.

Now we construct the generators $v_0, v_1, \ldots, v_g$, of a curve f of genus $g > 1$ with Puiseux characteristic $\beta_0, \beta_1, ..., \beta_g$. The intersection number of f with the $\hat{x}$ or $\hat{y}$ axis is given by the

equations $g(x,y) = x = 0$ or $g(x,y) = y = 0$, respectively. Then the corresponding orders of $g(\phi(t), \psi(t))$ are β_0 and β_1, for the intersections with the $\hat{x}$ and $\hat{y}$ axes, respectively, and the first two generators are $v_0 = \beta_0$ and $v_1 = \beta_1$. To calculate the next term, we consider the intersection between f and the leading order behavior $x = t^{\beta_0},\ y = t^{\beta_1}$ of the expansion (A2), which we define as the curve f_2. However, on account of $g > 1$, this parameterization contains a common factor $\mathrm{hcf}(\beta_0, \beta_1) = e_1 > 1$, which we must divide out to obtain the implicit representation $g(x,y) = x^{\beta_1/e_1} - y^{\beta_0/e_1}$ of f_2. It is the straightforward to calculate the series expansion of $g(\phi(t), \psi(t))$ to obtain

$$v_2 = i(f, f_2) = \mathrm{ord}(g(\phi(t), \psi(t))) = v_1 \frac{e_0}{e_1} + \beta_2 - \beta_1. \tag{A4}$$

Not giving any details, we can continue in this manner to find the remaining generators

$$v_{i+1} = \frac{e_{i-1}}{e_i} v_i + \beta_{i+1} - \beta_i, \quad i = 2, ..., g, \tag{A5}$$

the same number as the number of Puiseux exponents.

Finally, the semigroup is defined as $S(f) = \langle v_0, v_1, v_2, ..., v_g \rangle$, which is another invariant of the representation (A2), and thus of the curve. We state without proof that the number N_G of *gaps* of the semigroup determines the number of *self-intersections* (or double points) δ_f of the possible unfoldings of the curve. The number of gaps is half the conductor c of the semigroup, which is defined as the smallest member of $S(f)$ such that $c - 1$ is a gap. The conductor can be calculated from the intersection numbers, so that we obtain the general relation:

$$\delta_f = N_G = \frac{c}{2} = \frac{1}{2} \sum_{i=1}^{g} \left(\frac{e_{i-1}}{e_i} - 1 \right) v_i - v_0 + 1. \tag{A6}$$

To give two examples, consider $f : (x,y) = (t^3, t^7)$. The Puiseux characteristics are $\beta_0 = 3$ and $\beta_1 = 7$. The genus of the curve is $g = 1$, and so the semigroup is generated by the numbers $v_0 = 3$ and $v_1 = 7$. The conductor of the semigroup is $c = 12$, which is twice the number of gaps $G = \{1, 2, 4, 5, 8, 11\}$, so that the δ-invariant is $\delta_f = 6$. In the second example, we take $f : (x,y) = (t^4, t^6 + t^7)$. The characteristic of the curve is $\mathrm{ch}(f) = (4; 6, 7)$ and g=3. The semigroup is $S_f = \langle 4, 6, 13 \rangle$, the conductor $c = 16$, $\delta_f = 8$ and $G = \{1, 2, 3, 5, 7, 9, 11, 15\}$.

To complete the description of invariants of plane curve singularities, we describe the constraints on the possible values of the Zariski invariant λ, which we introduced before

in Subsection III C. Starting from a "good" parameterization (A2), $\lambda < \beta_2$ is the first monomial exponent above β_1. There can be a single such monomial only with $\beta_1 < \lambda \leq \beta_2$, and hence up to equivalence the germ of a plane curve singularity can be written in the form:

$$f: \quad x = t^{\beta_0}, \quad y = t^{\beta_1} + t^{\lambda} + \sum_{\beta_2 < i \leq c} c_i t^i. \tag{A7}$$

In particular, this shows that if one limits oneself to two exponents only, the Zariski invariant guarantees a complete classification of singularities. If there is a third monomial present, the singularity is modular, i.e. the coefficient c_i in front of this monomial cannot be reduced to unity. Since λ is not contained in the semigroup, it does not change the number of double points δ_f, but it reduces the codimension of the singularity.

The possible values λ can attain are subject to the conditions [32]:

$$\lambda, \lambda + v_0 \notin S(f) \quad \text{and} \quad v_1 < \lambda \leq \beta_2 = v_2 - v_1\big(\frac{v_1}{v_2} - 1\big). \tag{A8}$$

In particular, if $g = 1$, (A8) simplifies to

$$\lambda = n_1 v_1 - n_0 v_0, \quad n_0 \geq 2, \quad 2 \leq n_1 \leq v_1 - 1. \tag{A9}$$

Appendix B: Classification of singularities up to $m = 4$ with unfoldings

A complete classification of plane singularities does not exist, but one can consider singularities up to a certain order of the multiplicity m of the germ f. For historical reasons, singularities up to $m = 4$ are called simple singularities, whose classification we report now. The coefficients in front of the powers of the germ can all be normalized to unity, up to equivalence. We also report the miniversal unfolding F (when it is known explicitly), which contains parameters whose number equals the codimension.

1. A_{2k}, $m = 2$.

$$f: t \to (t^2, t^{2k+1}), \quad k \geq 1, \quad \operatorname{cod}(f)_{\mathcal{A}_e} = k,$$
$$F: \left(t^2, t^{2k+1} + \sum_{j=1}^{k} \mu_{2j-1} t^{2j-1}\right).$$

2. E_{6k}, $m = 3$.

(a) monomial:

$$f : t \to (t^3, t^{3k+1}), \quad k \geq 1, \quad \mathrm{cod}(f)_{\mathcal{A}_e} = 3k,$$
$$F : \left(t^3 + \epsilon_1 t, t^{3k+1} + \sum_{j=1}^{k} \mu_{3j-2} t^{3j-2} + \sum_{j=1}^{2k-1} \mu_{3j+1} t^{3j+1} \right).$$

(b) with Zariski invariant:

$$f : t \to (t^3, t^{3k+1} + (\pm)^{l-k} t^{3l+2}), \quad k \geq 2,\ k \leq l \leq 2k-2, \quad \mathrm{cod}(f)_{\mathcal{A}_e} = k + l + 1. \tag{B1}$$

3. E_{6k+2}, $m = 3$.

(a) monomial:

$$f : t \to (t^3, t^{3k+2}), \quad k \geq 1, \quad \mathrm{cod}(f)_{\mathcal{A}_e} = 3k + 1,$$
$$F : \left(t^3 + \epsilon_1 t, t^{3k+2} + \sum_{j=1}^{k} \mu_{3j-1} t^{3j-1} + \sum_{j=1}^{2k} \mu_{3j-2} t^{3j-2} \right).$$

(b) with Zariski invariant:

$$f : t \to (t^3,\ t^{3k+2} + (\pm)^{l-k} t^{3l+1}), \quad k \geq 2,\ k+1 \leq l < 2k-1, \quad \mathrm{cod}(f)_{\mathcal{A}_e} = k+l-1. \tag{B2}$$

4. $W_{1,2}$, $m = 4$.

(a) monomial:

$$f : t \to (t^4,\ \ t^5), \quad \mathrm{cod}(f)_{\mathcal{A}_e} = 6,$$
$$F : \left(t^4 + \epsilon_2 t^2 + \epsilon_1 t,\ \ t^5 + \mu_7 t^7 + \mu_3 t^3 + \mu_2 t^2 + \mu_1 t \right).$$

(b) with Zariski invariant:

$$f : t \to (t^4,\ \ t^5 \pm t^7), \quad \mathrm{cod}(f)_{\mathcal{A}_e} = 5,$$
$$F : \left(t^4 + \epsilon_2 t^2 + \epsilon_1 t,\ \ t^5 + \mu_3 t^3 + \mu_2 t^2 + \mu_1 t \right).$$

5. $W_{1,8}$, $m = 4$.

(a) monomial:

$$f : t \to (t^4, \quad t^7), \quad \mathrm{cod}(f)_{\mathcal{A}_e} = 9,$$
$$F : \left(t^4 + \epsilon_2 t^2 + \epsilon_1 t, \quad t^5 + \mu_{13} t^{13} + \mu_9 t^9 + \mu_6 t^6 + \mu_5 t^5 + \mu_3 t^3 + \mu_2 t^2 + \mu_1 t \right).$$

(b) with first Zariski invariant:

$$f : t \to (t^4, \quad t^7 \pm t^9), \quad \mathrm{cod}(f)_{\mathcal{A}_e} = 7,$$
$$F : \left(t^4 + \epsilon_2 t^2 + \epsilon_1 t, \quad t^5 + \mu_6 t^6 + \mu_5 t^5 + \mu_3 t^3 + \mu_2 t^2 + \mu_1 t \right).$$

(c) with second Zariski invariant:

$$f : t \to (t^4, \quad t^7 \pm t^{13}), \quad \mathrm{cod}(f)_{\mathcal{A}_e} = 8,$$
$$F : \left(t^4 + \epsilon_2 t^2 + \epsilon_1 t, \quad t^5 + \mu_9 t^9 + \mu_6 t^6 + \mu_5 t^5 + \mu_3 t^3 + \mu_2 t^2 + \mu_1 t \right).$$

6. $W^{\#}_{1,2k-1}$, $m = 4$, genus $g = 2$:

$$f : t \to (t^4, \quad t^6 + t^{2k+5}), \quad k \geq 1, \ k \geq 1, \quad \mathrm{cod}(f)_{\mathcal{A}_e} = k + 5,$$
$$F : \left(t^4 + \epsilon_2 t^2 + \epsilon_1 t, \quad t^6 + t^{2k+5} + \sum_{j=1}^{k+2} \mu_{2j-1} t^{2j-1} + \mu_2 t^2 \right).$$

ACKNOWLEDGMENTS

Funding through a Leverhulme Trust Research Project Grant is gratefully acknowledged

REFERENCES

[1] R. C. Caflisch and G. Papanicolau, eds., Singularities in fluids, plasmas and optics (Kluwer, 1993).

[2] A. L. Bertozzi, M. P. Brenner, T. F. Dupont, and L. P. Kadanoff, in Applied Mathematics Series Vol. 100, edited by L. Sirovich (Springer: New York, 1994) p. 155.

[3] L. P. Kadanoff, Phys. Today **50(9)**, 11 (1997).

[4] J. Eggers and M. A. Fontelos, Nonlinearity **22**, R1 (2009).

[5] J. Eggers and M. A. Fontelos, Singularities: Formation, Structure, and Propagation (Cambridge University Press, Cambridge, 2015).

[6] J. Eggers, Phys. Rev. Lett. **71**, 3458 (1993).

[7] C. G. Gibson, Singular points of smooth mappings (Pitman, 1979).

[8] V. I. Arnol'd, V. A. Vasil'ev, V. V. Goryunov, and O. V. Lyashko, in Dynamical Systems VI (Springer, Heidelberg, 1993).

[9] V. I. Arnol'd, V. A. Vasil'ev, V. V. Goryunov, and O. V. Lyashko, in Dynamical Syatems VIII (Springer, Heidelberg, 1993).

[10] Y. Lu, Singular theory and an introduction to catastrophre threory (Springer, 1976).

[11] G. M. Greuel, C. Lossen, and E. Shustin, Introduction to singularities and deformations (Springer, 2007).

[12] M. V. Berry, in Les Houches, Session XXXV, edited by R. Balian, M. Kleman, and J.-P. Poirier (North-Holland: Amsterdam, 1981) pp. 453–543.

[13] V. I. Arnold, Catastrophe Theory (Springer, 1984).

[14] V. I. Arnold, Mathematical methods of classical mechanics, second edition (Springer, 1989).

[15] V. I. Arnold, Singularities of caustics and wave fronts (Kluwer, 1990).

[16] M. S. Cramer and A. R. Seebass, J. Fluid Mech. **88**, 209 (1978).

[17] T. Poston and I. Stewart, Catastrophe Theory and Its Applications (Dover Publications, Mineola, 1978).

[18] B. Sturtevant and V. A. Kulkarny, J. Fluid Mech. **73**, 651 (1976).

[19] A. T. Cates and B. Sturtevant, Phys. Fluids **9**, 3058 (1997).

[20] J. Eggers and M. A. Fontelos, Panoramas et Synthèses **38**, 69 (2013).

[21] J.-T. Jeong and H. K. Moffatt, J. Fluid Mech. **241**, 1 (1992).

[22] P. Doshi, I. Cohen, W. W. Zhang, M. Siegel, P. Howell, O. A. Basaran, and S. R. Nagel, Science **302**, 1185 (2003).

[23] R. Gilmore, Catastrophe theory for scientists and engineers (Interscience, 1981).

[24] D. T. Papageorgiou, Phys. Fluids **7**, 1529 (1995).

[25] J. Eggers, Rev. Mod. Phys. **69**, 865 (1997).

[26] J. Eggers, Phys. Fluids **24**, 072103 (2012).

[27] J. Montaldi, "Singularities, bifurcations, and catastrophe," Lecture Notes (2012).

[28] C. T. C. Wall, Singular points of plane curves (Cambridge, 2004).

[29] J. W. Bruce and P. J. Giblin, Curves and singularities (Cambridge University Press, 1992).

[30] E. Casas-Alvero, Singularities of plane curves (Cambridge, 2000).

[31] M. E. Hernandes, M. E. R. Hernandes, and M. A. S. Ruas, Cadernos de Maremática **7**, 155 (2006).

[32] V. Bayer and A. Hefez, Bol. Soc. Bras. Mat. **32**, 63 (2001).

[33] K.-I. Nishiyama and M. Watari, Arch. Math. **86**, 529 (2006).

[34] O. Zariski, PNAS **56**, 781 (1966).

[35] A. Hefez and M. E. Hernandes, J. Symb. Comp. **44**, 624 (2009).

[36] A. Hefez and M. E. Hernandes, Bull. London Math. Soc **43**, 289 (2011).

[37] M. Z. Bazant and D. Crowdy, in Handbook of Materials Modeling, edited by S. Yip (Springer, 2005) p. 1417.

[38] L. D. Landau and E. M. Lifshitz, Mechanics (Pergamon: Oxford, 1976).

[39] V. Arnold, Russian Math. Survays **38**, 87 (1983).

[40] M. Born and E. Wolf, Principles of Optics (Oxford, Pergamon, 1980).

[41] A. Chorin and J. E. Marsden, A Mathematical Introduction to Fluid Mechanics (Springer, 2000).

[42] G. B. Whitham, Linear and Nonlinear Waves (John Wiley & Sons, 1974).

[43] G. B. Whitham, J. Fluid Mech. **2**, 145 (1957).

[44] W. D. Henshaw, N. F. Smyth, and D. W. Schwendeman, J. Fluid Mech. **171**, 519 (1986).

[45] D. W. Schwendeman, in Proc. 20th Int. Symp. on Shock Waves, edited by B. Sturtevant, J. E. Shepherd, and H. G. Hornung (World Scintific, Singapore, 1995) pp. 531–536.

[46] D. W. Schwendeman and G. B. Whitham, Proc. R. Soc. Lond. A **413**, 297 (1987).

[47] J. Eggers, M. A. Fontelos, and N. Suramlishvili, preprint (2016).

[48] P. Y. Polubarinova-Kochina, Dokl. Akad Nauk USSR **47**, 254 (1945).

[49] P. Y. Polubarinova-Kochina, Prikl. Matem. Mech. **9**, 79 (1945).

[50] L. A. Galin, Dokl. Akad. Nauk. SSSR **47**, 246 (1945).

[51] B. Gustafsson and A. Vasil'ev, Conformal and potential analysis in Hele-Shaw cells (Birkhäuser, 2006).

[52] L. J. Cummings and S. D. Howison, Euro. J. Appl. Math. **10**, 681 (1999).

[53] S. Richardson, J. Fluid Mech. **33**, 476 (1968).

[54] L. J. Cummings, S. D. Howison, and J. R. King, Phys. Fluids **9**, 477 (1997).

[55] J.-T. Jeong, Eur. J. Mech. B/Fluids **26**, 720 (2007).

[56] J.-T. Jeong, Phys. Fluids **11**, 521 (1999).

[57] J.-T. Jeong, Phys. Fluids **22**, 082102 (2010).

[58] L. K. Antanovskii, J. Fluid Mech. **327**, 325 (1996).

[59] D. Crowdy, J. Engin. Math. **44**, 311 (2002).

[60] E. Lorenceau, F. Restagno, and D. Quéré, Phys. Rev. Lett. **90**, 184501 (2003).

[61] R. W. Hopper, J. Fluid Mech. **213**, 349 (1990).

[62] R. W. Hopper, J. Fluid Mech. **230**, 355 (1991).

[63] R. W. Hopper, J. Fluid Mech. **243**, 171 (1992).

[64] R. W. Hopper, Q. J. Mech. appl. Math. **46**, 193 (1993).

[65] S. Richardson, Euro. Jnl. Appl. Math. **3**, 193 (1992).

[66] S. Tanveer and G. L. Vasconcelos, J. Fluid Mech. **301**, 325 (1995).

[67] D. Crowdy, Eur. J. Appl. Math. **14**, 421 (2003).

[68] D. Crowdy, J. Fluid Mech. **476**, 345 (2003).

[69] G. K. Batchelor, An Introduction to Fluid Dynamics (Cambridge University Press, Cambridge, 1967).

[70] A. E. H. Love, Proc. Camb. Phil. Soc. **7**, 175 (1891).

[71] B. Hopkinson, Proc. Lond. Math. Soc. **29**, 142 (1898).

[72] A. Craya, La Houille Blanche **4**, 44 (1949).

[73] C. Sautreaux, J. Math. Pures Appl. **7**, 125 (1901).

[74] C. R. Dun and G. C. Hocking, J. Engin. Math. **29**, 1 (1995).

[75] G. D. Crapper, J. Fluid Mech. **2**, 532 (1957).

[76] W. Kinnersley, J. Fluid Mech. **77**, 229 (1976).

[77] DLMF, "NIST Digital Library of Mathematical Functions," http://dlmf.nist.gov/, Release 1.0.9 of 2014-08-29, online companion to [85].

[78] S. Wrigge, Math. Comp. **37**, 495 (1981).

[79] J. Eggers, M. A. Fontelos, D. Leppinen, and J. H. Snoeijer, Phys. Rev. Lett. **98**, 094502 (2007).

[80] M. V. Berry, in Singular Optics, edited by E. Soskin and M. S. Frunzenskoe (Crimea, SPIE, 1998) pp. 1–5.

[81] J. Nye, Natural Focusing and Fine Structure of Light: Caustics and Wave Dislocations (Institute of Physics Publishing, Bristol, 1999).

[82] J. Eggers, J. Hoppe, M. Hynek, and N. Suramlishvili, Geometric Flows **1**, 17 (2014).

[83] T. Grava, C. Klein, and J. Eggers, Nonlinearity **29**, 1384 (2016).

[84] J. Eggers and T. Grava, (2016).

[85] F. W. J. Olver, D. W. Lozier, R. F. Boisvert, and C. W. Clark, eds., NIST Handbook of Mathematical Functions (Cambridge University Press, New York, NY, 2010) print companion to [77].